

LOW-MASS X-RAY BINARIES AND GLOBULAR CLUSTERS IN EARLY-TYPE GALAXIES. I. CHANDRA OBSERVATIONS

PHILIP J. HUMPHREY¹ AND DAVID A. BUOTE¹

Submitted to the Astrophysical Journal

ABSTRACT

We present a *Chandra* survey of LMXBs in 24 early-type galaxies. Correcting for detection incompleteness, the X-ray luminosity function (XLF) of each galaxy is consistent with a powerlaw with negative logarithmic differential slope, $\beta \sim 2.0$. However, β strongly correlates with incompleteness, indicating the XLF flattens at low- L_X . The composite XLF is well-fitted by a powerlaw with a break at $(2.21^{+0.65}_{-0.56}) \times 10^{38} \text{ erg s}^{-1}$ and $\beta = 1.40^{+0.10}_{-0.13}$ and $2.84^{+0.39}_{-0.30}$ below and above it, respectively. The break is close to the Eddington limit for a $1.4M_{\odot}$ neutron-star, but the XLF shape rules out its representing the division between neutron-star and black-hole systems. Although the XLFs are similar, we find evidence of some variation between galaxies. The high- L_X XLF slope does not correlate with age, but may correlate with $[\alpha/\text{Fe}]$. Considering only LMXBs with $L_X > 10^{37} \text{ erg s}^{-1}$, matching the LMXBs with globular clusters (GCs) identified in *HST* observations of 19 of the galaxies, we find the probability a GC hosts an LMXB is proportional to $L_{GC}^{\alpha} Z_{Fe}^{\gamma}$ where $\alpha = 1.01 \pm 0.19$ and $\gamma = 0.33 \pm 0.11$. Correcting for GC luminosity and colour effects, and detection incompleteness, we find no evidence that the fraction of LMXBs with $L_X > 10^{37} \text{ erg s}^{-1}$ in GCs (40%), or the fraction of GCs hosting LMXBs ($\sim 6.5\%$) varies between galaxies. The spatial distribution of LMXBs resembles that of GCs, and the specific frequency of LMXBs is proportional to the GC specific luminosity, consistent with the hypothesis that all LMXBs form in GCs. If the LMXB lifetime is τ_L and the duty cycle is F_d , our results imply $\sim 1.5(\tau_L/10^8 \text{ yr})^{-1} F_d^{-1}$ LMXBs are formed Gyr^{-1} per GC and we place an upper limit of 1 active LMXB in the field per $3.4 \times 10^9 L_{\odot}$ of V-band luminosity.

Subject headings: Xrays: galaxies—galaxies: elliptical and lenticular, cD—Xrays: binaries—galaxies: star clusters

1. INTRODUCTION

As the end-points of stellar evolution, studies of X-ray binary (XRB) populations provide a valuable insight not only into black-hole and neutron-star demographics but also into the history of star-formation within galaxies. In the four decades since the discovery of Sco X-1 (Giacconi et al. 1962), generations of X-ray satellites have revealed a rich variety of phenomenology in the ~ 300 XRBs in the Milky Way (White et al. 1995; Liu et al. 2000, 2001). Unfortunately, studies of these objects are hampered by a number of factors such as uncertainty in the distances to (and hence luminosities of) Galactic sources, the limited numbers of sources and the mixture of old and young stellar populations in the Milky Way, which can make isolating different influences on the population challenging. These problems can, in part, be mitigated through observations of external, early-type galaxies, which comprise a clean old stellar population and XRBs all at essentially the same distance. The absence of massive, young stars in these systems means that their XRB populations are entirely comprised of low-mass X-ray binaries (LMXBs).

Prior to the launch of *Chandra* only a small number of the very brightest point-sources in early type galaxies could be resolved from the diffuse galactic emission (Fabbiano 1989). *Chandra*'s advent revolutionized this picture, enabling LMXBs to be resolved in large numbers and studied directly (e.g. Sarazin et al. 2001; Blanton et al. 2001; Humphrey & Buote 2004; Humphrey et al.

2003; Fabbiano 2006, for a recent review). Of particular interest are the X-ray luminosity functions (XLFs) of the XRBs, which in principle may provide vital clues as to the way in which the sources form and evolve (e.g. Belczynski et al. 2004; Ivanova & Kalogera 2006). In star-forming galaxies, for example, the high-mass X-ray binary population dominates the XLF, making it much flatter than is typical of LMXBs in the Milky Way or early-type galaxies (Kilgard et al. 2002; Colbert et al. 2004; Grimm et al. 2003). Between early-type galaxies, the XLF appears remarkably similar (Kim & Fabbiano 2004; Gilfanov 2004), although there is some debate regarding its precise functional form. Various authors have parameterized it as a steeply falling broken powerlaw with a break around $2-4 \times 10^{38} \text{ erg s}^{-1}$ and a high-luminosity negative logarithmic differential slope, $\beta \simeq 2-3$ (Sarazin et al. 2000; Kraft et al. 2001; Colbert et al. 2004), and there may be evidence of a second break at $\sim 2 \times 10^{37} \text{ erg s}^{-1}$ (e.g. Gilfanov 2004). Alternatively, the XLF has also been modeled as a single powerlaw, truncated above some limit (Sivakoff et al. 2003; Jordán et al. 2004). Kim & Fabbiano (2003) argued that the presence of a break in the powerlaw XLF of NGC 1316 can be artificially induced by source detection incompleteness effects, after correcting for which the data were consistent with a single powerlaw XLF. We obtained a similar result for the lenticular galaxy NGC 1332 (Humphrey & Buote 2004). Applying an incompleteness correction to a sample of ~ 15 early-type galaxies, Kim & Fabbiano (2004) also reproduced this result, but they reported marginal evidence of a break at $5 \times 10^{38} \text{ erg s}^{-1}$

¹ Department of Physics and Astronomy, University of California at Irvine, 4129 Frederick Reines Hall, Irvine, CA 92697-4575

when the data for all the galaxies were combined.

Although the presence of the upper break is controversial, its luminosity is suggestively close to the Eddington limit of a $1.4 M_{\odot}$ neutron star ($L_{\text{EDD}} = 2-4 \times 10^{38} \text{ erg s}^{-1}$, depending on the composition of the accreting matter and the neutron-star equation of state: Paczyński 1983), leading to suggestions that it may delineate the division between neutron-star and black-hole accretors (Sarazin et al. 2001). Kim & Fabbiano (2004), however, argued that the break in their data was at too high a luminosity to make this explanation tenable. Similarly, in the elliptical galaxy NGC 720, Jeltema et al. (2003) reported a break at $\sim 1 \times 10^{39} \text{ erg s}^{-1}$, which they speculated may relate to a young stellar population born in putative recent merger activity. Bildsten & Deloye (2004) argued that if all bright LMXBs in early-type galaxies are ultra-compact binaries with He or C/O-rich donor stars, this might explain both the break and the low-luminosity slope of the XLF found by Kim & Fabbiano (2004).

Another issue for which studies of early-type galaxies are useful is the role of globular clusters (GCs) in forming LMXBs. It has long been recognized that there is an over-density of LMXBs per unit optical light within Milky Way GCs as compared to the field, indicating that dynamical processes within them play an important role in efficient LMXB formation (Fabian et al. 1975; Clark 1975). Since there are only ~ 150 GCs in the Milky Way, however, there are insufficient sources to examine this relationship in detail. In contrast, many early-type galaxies host rich GC populations (e.g. Gebhardt & Kissler-Patig 1999; Kundu & Whitmore 2001), providing ideal laboratories in which to investigate the LMXB-GC connection. Using *ASCA* data, White et al. (2002) found a strong correlation between the specific frequency of globular clusters (S_N) in a sample of 8 early-type galaxies and the integrated luminosity of LMXBs, inferred from spectral-fitting, leading them to suggest that all LMXBs within the galaxies were formed in GCs. With *Chandra* it has become possible to isolate individual LMXBs associated with GCs and to study the populations of sources individually. The reported fraction of LMXBs associated with GCs varies from $\sim 20-70\%$ (e.g. Angelini et al. 2001; Humphrey & Buote 2004; Kundu et al. 2002; Xu et al. 2005; Blanton et al. 2001). Using a sample of 4 galaxies Sarazin et al. (2003) suggested this fraction varies along the Hubble sequence, possibly reflecting the increase in S_N from spiral to elliptical galaxies, and perhaps indicating different populations of LMXBs which form in the field and in GCs. Irwin (2005) and Juett (2005) reported further evidence that the fraction depends on S_N . Irwin also argued that the total luminosity of the LMXBs is not strictly proportional to S_N , which would imply a significant fraction of sources, even in early-type galaxies, forms in the field. The strength of the Juett correlation, however, has been called into question by Kim et al. (2006b).

Another way to address this question is to compare the spatial distributions of LMXBs and GCs, which has been attempted by Kim et al. (2006b) and Kundu et al. (2007, which was made publicly available after we submitted this present work), for small samples of galaxies (6 and 5, respectively). However, these studies have produced inconsistent results, which may reflect the small-number

statistics of the samples. Kim et al. (2006b) found that the radial distribution of GCs hosting LMXBs is significantly steeper than that of the GC population, but similar to the distribution of LMXBs as a whole, and to the optical light. They argued this may indicate that dynamical processes affecting GCs close to the centres of each galaxy may trigger LMXB production. In contrast, Kundu et al. (2007) found that the radial distribution of GCs hosting an LMXB is similar to the GC population as a whole, and significantly flatter than the LMXB population, which they argued hinted at significant formation in the field.

Based on small samples of a handful of galaxies, it has been shown that approximately 4% of GCs are found to host active LMXBs (Angelini et al. 2001; Kundu et al. 2002, 2003; Sarazin et al. 2003). Using a sample of 6 elliptical galaxies Kim et al. (2006b) found evidence that this fraction varies considerably from galaxy to galaxy. There is no evidence that the properties of LMXBs in GCs systematically differ from those in the field. In contrast, GCs which are brighter or redder are systematically more likely to contain an LMXB (Angelini et al. 2001; Kundu et al. 2002, 2003; Sarazin et al. 2003; Kim et al. 2006b; Smits et al. 2006; Sivakoff et al. 2007). The luminosity dependence appears approximately consistent with the probability that a GC contains an LMXB being exactly proportional to its luminosity (e.g. Sarazin et al. 2003; Smits et al. 2006), although Sivakoff et al. (2007), based on a sample of 11 Virgo galaxies, argued that the dependence upon mass is slightly stronger.

The colour-dependence is indicative of a metallicity effect (e.g. Kundu et al. 2003), and a number of authors have proposed possible explanations (for a review, see Jordán et al. 2004). Maccarone et al. (2004) proposed a model in which the effect arises due to the balance of mass transfer through irradiation-induced winds and Roche lobe overflow systematically varying from metal-poor to metal-rich systems. In this picture, LMXBs associated with blue GCs should exhibit significant intrinsic absorption. However, Kim et al. (2006b) reported no evidence of spectral differences between sources in red and in blue GCs. Other possible explanations include the effect of metallicity on the stellar mass-radius relation (Bellazzini et al. 1995, although this may not be sufficiently large an effect: Maccarone et al. 2004), variation in the stellar initial mass function (IMF) with the GC metallicity (Grindlay 1987, although see Kroupa 2002) or the absence of a deep convective zone in metal-poor stars impeding magnetic braking, and hence LMXB formation (Ivanova 2006, although it is not clear if this model would produce the observed power-law dependence of LMXB incidence on the GC metallicity).

To date the LMXB-GC connection has only been investigated with small galaxy samples, making it hard to draw strong conclusions about the relation between them in general. In particular the fraction of LMXBs which may be formed in the field is very uncertain. In addition, the presence of a break in the XLF remains controversial. The investigation of the LMXBs in a larger sample of galaxies is therefore vital to provide a clearer insight into the processes which give rise to them. In this paper, we investigate the LMXB population of 24 early-type galaxies observed with *Chandra* and *HST*, focusing on both the XLF and the LMXB-GC connection.

This work is also part of a series investigating the X-ray properties of a sample of galaxies. In our previous papers we have addressed the metal content of the ISM and their mass profiles (Humphrey & Buote 2006; Humphrey et al. 2006). We consider here only a subset of the galaxies which yield interesting constraints on the LMXB populations. In addition, we include the nearby galaxy NGC 1404, the diffuse emission of which is difficult to disentangle from that of the Fornax “cluster” but which has a fairly rich LMXB and GC population. The galaxies and a summary of their properties, and the *Chandra* observations used, are listed in Table 1. In a companion paper, Humphrey (2008, hereafter Paper II), we present the *HST* data-reduction and analysis upon which we build here. Of the 24 galaxies in the sample, 7 were included in the Kim & Fabbiano (2004) study of the XLF, 3 in the sample of Kim et al. (2006b), who considered the LMXB-GC connection, 4 in the Smits et al. (2006) sample, and 3 in the Sarazin et al. (2003) sample. All errors quoted in this paper are 90% confidence limits unless otherwise stated.

2. OBSERVATIONS AND DATA ANALYSIS

For data reduction, we used the *CIAO* 3.3.0.1 and *Heasoft* 6.0 software suites, in conjunction with *Chandra* calibration database (*Caldb*) version 3.2.1. Spectral-fitting was conducted with *Xspec* 11.3.2p. In order to ensure the most up-to-date calibration, all data were reprocessed from the “level 1” events files, following the standard *Chandra* data-reduction threads². Bad-pixel maps were created using the *CIAO* tool *acis_run_hotpix*. We applied the standard correction to take account of the time-dependent gain-drift and, for those galaxies observed with ACIS-I, we applied the standard CTI correction as implemented in the standard *CIAO* tools.

To identify periods of enhanced background (“flaring”), which seriously degrades the signal-to-noise (S/N) we accumulated background lightcurves for each exposure from low surface-brightness regions of the active chips. We excluded obvious diffuse emission and data in the vicinity of any detected point-sources (see below). Periods of flaring were identified by eye and excised. The final exposure times are listed in Table 1.

Point source detection was performed using the *CIAO* tool *wavdetect* (Freeman et al. 2002). Point sources were identified in full-resolution images of the *ACIS* focal-plane containing, where appropriate, the S3 chip and any other chips onto which the B-band twenty-fifth magnitude (D_{25}) ellipse listed in the Third Catalogue of Bright Galaxies (de Vaucouleurs et al. 1991, hereafter RC3) extends. For ACIS-I observations, all of the ACIS-I chips were considered. To maximise the likelihood of identifying sources with peculiarly hard or soft spectra, images were created in three energy bands, 0.1–10.0 keV, 0.1–3.0 keV and 3.0–10.0 keV. Sources were detected separately in each image. In order to minimize spurious detections at node or chip boundaries we supplied the detection algorithm with exposure-maps generated at energies 1.7 keV, 1.0 keV and 7 keV respectively (although the precise energies chosen should make little difference to the results). The detection algorithm searched for structure over pixel-scales of 1, 2, 4, 8 and 16 pixels,

and the detection threshold was set to 10^{-6} , implying ~ 1 spurious detection due to background fluctuations per CCD. The source-lists obtained in each energy-band were combined and duplicated sources removed, and the final list was checked by visual inspection of the images. For each source, we obtained radial surface brightness profiles, as described in Humphrey & Buote (2004), which we examined to ensure that only point-like sources were considered (where there were sufficient photons). This led to the elimination of central sources in many of the galaxies, which were spuriously detected by the algorithm due to a centrally-peaked surface brightness profile. In a few other cases (notably in the centre of NGC 5846), other “sources” eliminated in this way appeared to be associated with compact knots of X-ray emission, or the sharp edges of X-ray structures. The spiral galaxy NGC 4647 is projected onto the part of the image of NGC 4649, possibly contaminating our source list for this object. In order to minimize such contamination, we excluded all point-sources which lay within the D_{25} ellipse of NGC 4647 from further analysis.

Spectra were extracted for each source from the 3σ source regions returned by the detection algorithm. We note that there was very little problem of these regions overlapping; in the few cases where they were found to overlap, the regions were slightly shrunk to minimize likelihood of contamination, but this should not strongly affect the measured fluxes. For each source spectra and spectral responses were generated using the standard *CIAO* tools and local background regions were chosen from which background products were similarly extracted. The background regions were chosen to cover an area at least 8 times the source region, and containing at least 50 photons, and excluding data from the 6σ detection region of *all* detected sources. Furthermore, we restricted the background regions to lie entirely on the same chip and CCD node as the source centroid. A few sources were eliminated at this stage as they contained no (background-subtracted) photons; these are most likely spurious detections due to background fluctuations. Complete lists of the detected sources which lie within D_{25} are given in the Appendix.

3. X-RAY SOURCE PROPERTIES

3.1. Hardness ratios

Individual point-sources typically contained too few background-subtracted photons to enable full spectral-fitting. Therefore to obtain a crude insight into their spectral properties, we computed spectral hardness ratios (see e.g. Kilgard et al. 2002; Humphrey et al. 2003). We defined HR1 and HR2 for each source as, respectively, $HR1 = (S-M)/(S+M)$ and $HR2 = (M-H)/(M+H)$, where S is the background subtracted count-rate in the band 0.3–1.5 keV, M is the count-rate in the band 1.5–3.0 keV and H corresponds to 3.0–5.0 keV. Fig 1 shows, for a sub-sample of the galaxies, plots of the hardness ratios for those sources with more than 50 photons. For comparison purposes, we also show the loci in the HR2–HR1 plane of a simple absorbed powerlaw as N_H and Γ are allowed to vary. The exact positions of these grids do not vary substantially between observations.

Most of the sources are consistent with having low column densities (for typical Galactic line-of-sight N_H val-

² <http://cxc.harvard.edu/ciao/threads/index.html>

TABLE 1
TARGET LIST AND OBSERVATION LOG

Name	Type	Dist Mpc	D ₂₅ '	L _K 10 ¹¹ L _⊙	Age Gyr	[Fe/H]	[α/Fe]	Obsid	Inst	Date dd/mm/yy	Exp ks
IC4296	E-Radio-gal	50.8	3.8	5.2	12.	-0.10 ± 0.07	0.31 ± 0.05	3394	S	10/09/01	25.
NGC720	E5	25.7	4.6	1.7	2.9 ^{+0.8} _{-0.2}	0.17 ± 0.13	0.37 ± 0.03	492	S	12/10/00	29.
NGC1332	S(s)0	21.3	4.1	1.4	4.1 ^{+5.4} _{-0.9}	-0.15 ± 0.14	0.31 ± 0.10	4372	S	19/09/02	45.
NGC1387	SAB(s)0	18.9	3.3	0.78	4168	I	20/05/03	45.
NGC1399	cD;E1pec	18.5	6.9	2.1	12. ± 2.	-0.11 ± 0.08	0.37 ± 0.03	319	S	18/01/00	56.
NGC1404	E1	19.5	4.1	1.5	12. ^{+2.} _{-3.}	-0.28 ± 0.09	0.25 ± 0.03	2942	S	13/02/03	29.
NGC1407	E0	26.8	5.3	3.1	12. ± 1.	-0.18 ± 0.05	0.33 ± 0.01	791	S	16/08/00	40.
NGC1549	E0-1	18.3	4.7	1.3	5.1 ± 0.4	-0.10 ± 0.04	0.240 ± 0.006	2077	S	08/11/00	22.
NGC1553	SA(rl)0;LINER	17.2	5.3	1.9	5.7 ^{+0.7} _{-0.5}	0.23 ± 0.02	0.170 ± 0.006	783	S	02/01/00	14.
NGC3115	S0	9.00	7.3	0.74	15. ± 3.	0.030 ± 0.10	0.11 ± 0.07	2040	S	14/06/01	36.
NGC3585	E7/S0	18.6	6.1	1.5	10. ^{+3.} _{-4.}	-0.13 ± 0.11	0.20 ± 0.07	2078	S	03/06/01	35.
NGC3607	SA(s)0	21.2	4.5	1.5	15. ^{+2.} _{-2.}	-0.13 ± 0.11	0.19 ± 0.07	2073	I	12/06/01	38.
NGC3923	E4-5	21.3	6.4	2.3	3.3 ^{+0.4} _{-0.2}	0.13 ± 0.06	0.34 ± 0.02	1563	S	14/06/01	8.8.
NGC4125	E6pec;Liner	22.2	5.8	1.8	13. ± 5.	-0.39 ± 0.17	0.33 ± 0.10	2071	S	09/09/01	63.
NGC4261	E2-3;Liner;Sy3	29.3	4.1	2.2	15.0 ± 0.6	-0.21 ± 0.06	0.25 ± 0.01	834	S	06/05/00	34.
NGC4365	E3	19.0	5.8	1.6	3.9 ^{+5.9} _{-0.7}	-0.020 ± 0.12	0.19 ± 0.09	2015	S	02/06/01	40.
NGC4472	E2/S0(2);Sy2	15.1	9.7	3.2	9.0 ± 1.2	-0.0100 ± 0.12	0.16 ± 0.02	321	S	12/06/00	32.
NGC4494	E1-2;LINER	15.8	4.5	0.81	15. ± 5.	-0.24 ± 0.12	0.16 ± 0.08	2079	S	05/08/01	15.
NGC4552	E;LINER-HII	14.3	5.0	0.85	12. ± 1.	-0.050 ± 0.061	0.24 ± 0.01	2072	S	22/04/01	54.
NGC4621	E5	17.0	5.0	1.2	7.1 ^{+4.8} _{-2.3}	-0.030 ± 0.11	0.28 ± 0.09	2068	S	01/08/01	25.
NGC4649	E2	15.6	7.4	2.4	13. ± 1.	0.050 ± 0.085	0.25 ± 0.01	785	S	20/04/00	21.
NGC5018	E3	42.6	3.6	3.0	2.0 ^{+1.4} _{-0.2}	0.15 ± 0.17	0.0100 ± 0.085	2070	S	14/04/01	28.
NGC5845	E	24.0	0.90	0.27	12.	-0.12 ± 0.16	0.26 ± 0.10	4009	S	03/01/03	30.
NGC5846	E0-1;LINER-HII	21.1	3.8	1.5	15. ± 1.	-0.18 ± 0.10	0.22 ± 0.01	788	S	24/05/00	23.

NOTE. — Target list and observation details. All distances (Dist) are taken from Tonry et al. (2001), corrected for the the new Cepheid zero-point (Jensen et al. 2003), except for IC 4296, taken from Jensen et al. (2003), and NGC 5018 from D_n-σ relation (Faber et al. 1989). B-band twenty-fifth magnitude isophote (D₂₅) diameters are taken from RC3. K-band luminosities (L_K) were taken from 2MASS (Jarrett 2000), adopting M_K = 3.41. We report the age of the stellar population, its metallicity, [Fe/H] and its α-to-Fe ratio, [α/Fe] (see §6.1.3), and their 1-σ errors. The *Chandra* observation identifier is given (ObsID), as is the ACIS instrument (inst), the date of the observation start and the total exposure (exp), having cleaned the data to remove flaring (see text).

ues the grid lines are practically indistinguishable from the $N_{\mathrm{H}}=0$ case), and powerlaw slopes, $\Gamma \sim 1-3$. Such parameters are as expected for an LMXB population in an early-type galaxy (see e.g. Humphrey et al. 2003). A small number of sources exhibit much harder colours, implying intrinsic absorption. Some or all of these objects may be heavily-absorbed background AGN. We do not exclude such objects from subsequent analysis, since we explicitly take account of the expected numbers of background sources.

3.2. Fluxes

Since direct spectral fitting was impractical, it was necessary to adopt a canonical model for the spectrum to obtain a flux estimate for each source. We adopted a simple powerlaw model, with $\Gamma = 1.55$, which has been shown to fit adequately the composite spectra of detected LMXBs (Irwin et al. 2003, see also § 3.3), and modified by photoelectric absorption due to the Galactic ISM along the line-of-sight (Dickey & Lockman 1990). Such a model is broadly consistent with the source hardness ratios (§ 3.1) and models of a similar shape have also been fitted to the spectra of LMXBs within the Milky Way (e.g. Church & Baucińska-Church 2001). This model was folded through the response matrices generated at each source position, and used to infer a counts-to-flux conversion ratio in the 0.3–7.0 keV band. The 0.3–7.0 keV background-subtracted fluxes of each source were extracted from the regions defined from which to extract spectra. Although a small number of sources ap-

pear heavily absorbed (§ 3.1), and so this count-to-flux conversion ratio is not formally correct, the X-ray luminosity function we adopt to account for interlopers (§ 4.2) similarly does not incorporate the intrinsic absorption in estimating the flux, and so the results are self-consistent. Given the narrow band in which we compute fluxes, by definition, they underestimate the bolometric flux of the source. However, the extrapolation of the spectrum outside the adopted band is highly uncertain and so we compute the XLF of the sources for this narrow band. The luminosities are shown for each source in the Appendix.

3.3. Composite spectra

With a sample of 15 galaxies, Irwin et al. (2003) showed that the composite spectrum of all the detected LMXBs is featureless and can be well-fitted by simple empirical models such as a powerlaw with $\Gamma = 1.56$ or thermal bremsstrahlung with kT=7.3 keV. In order to test this with our sample, for each galaxy, we accumulated composite source and background spectra for all of the observed sources which lie within D₂₅, excluding the central ∼20'' (where background subtraction may be more problematical). These spectra were added in count-rate space, having first scaled the background spectra by the ratio of the source to background BACKSCAL keywords. The response matrices were averaged together with the *Heasoft* tools `addrmf` and `addirf` and adopting the background-subtracted count-rate of each corresponding spectrum as a weighting factor.

We fitted the composite spectrum in the range 0.5–

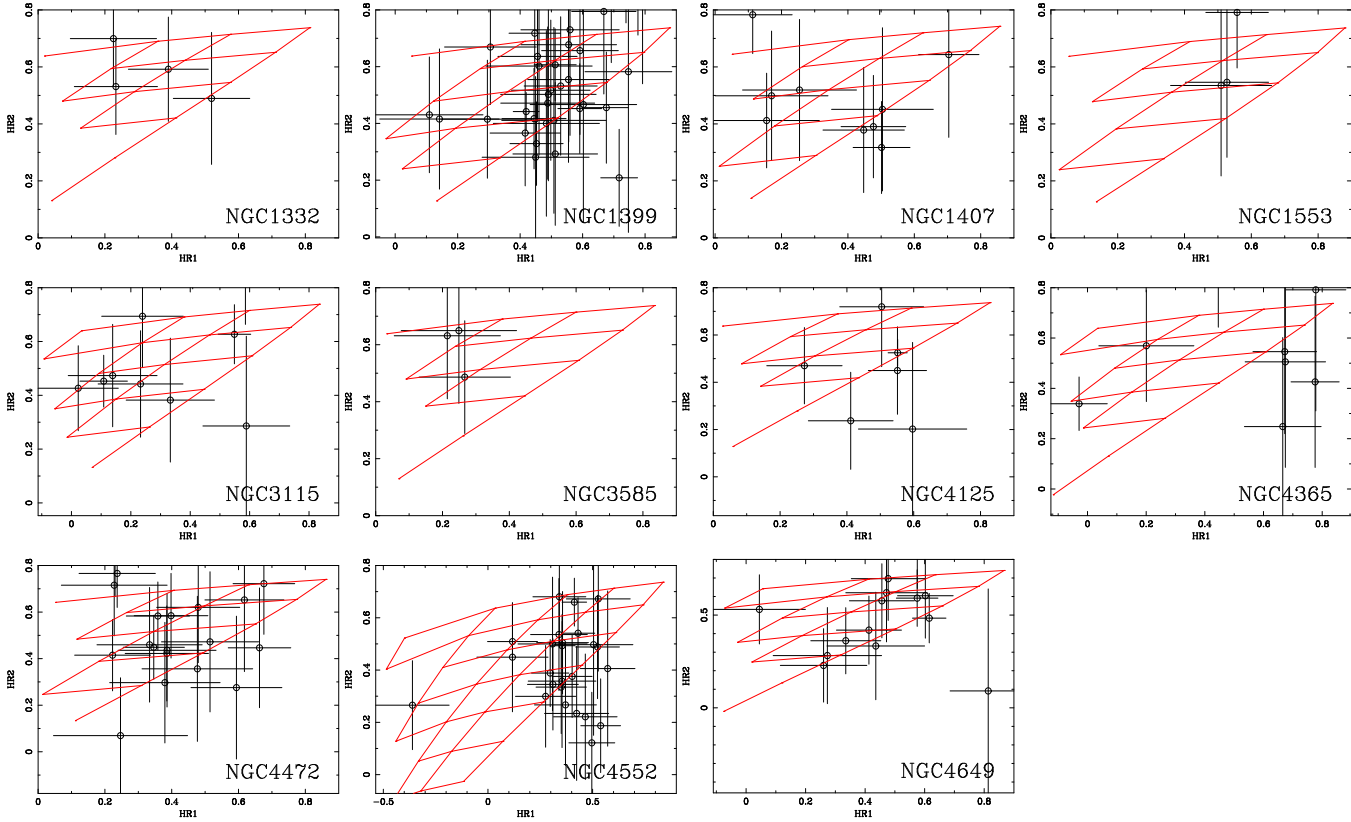


FIG. 1.— Hardness ratio plots of point sources with more than 50 photons for a subsample of the galaxies. The definitions of the hardness ratios HR1 and HR2 are given in the text. Also shown is a grid of loci in the colour-colour plane for a simple photo-absorbed powerlaw as N_{H} and Γ are allowed to vary. N_{H} increases to the left and grid lines are shown for $N_{\text{H}}=0.0, 0.25, 0.5, 1.0, 2.0, 4.0$ and $8.0 \times 10^{22} \text{ cm}^{-2}$. Γ increases upwards, with grid lines shown for $\Gamma=0.0-3.0$, in steps of 0.5

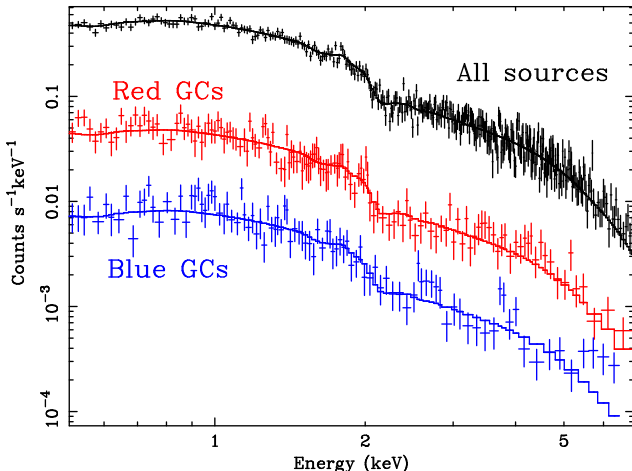


FIG. 2.— Composite spectra of the LMXBs (upper spectrum; black), folded through the instrumental response. The data are shown fitted with an absorbed bremsstrahlung model, with kT fixed at 7.3 keV. Also shown are the composite spectrum of LMXBs associated with red GCs and, scaled for clarity by a factor 0.3, that of LMXBs associated with blue GCs (§5.4.2). These spectra are shown fitted with the same bremsstrahlung model.

7.0 keV, having first rebinned it to ensure S/N of 3 in each bin, and at least 20 photons (to allow the use of the χ^2 fitting statistic). We fitted the spectrum using Xspec. The spectrum is remarkably featureless (Fig 2) and well-fitted by a single, absorbed powerlaw ($\chi^2/\text{dof}=354/339$), with $\Gamma = 1.68 \pm 0.04$ and $N_{\text{H}} = (7.5 \pm 1.1) \times 10^{20} \text{ cm}^{-2}$. If we fitted the data, instead, with a bremsstrahlung model,

we obtained a similarly good fit ($\chi^2/\text{dof}=357/339$), with $kT=7.8_{-0.7}^{+0.8}$ and $N_{\text{H}}=(2.1 \pm 0.08) \times 10^{20} \text{ cm}^{-2}$. These results are consistent with Irwin et al. (2003), although Γ is slightly larger for the powerlaw case. It is interesting to note that N_{H} obtained for the bremsstrahlung case is in better agreement with the average Galactic line-of-sight column density for the galaxies in our sample ($\sim 3 \times 10^{20} \text{ cm}^{-2}$) (see Humphrey & Buote 2006), implying it is more representative. Fitting this model to the composite source spectra accumulated for each galaxy individually, with N_{H} fixed to the nominal value for the appropriate Galactic line-of-sight, we obtained acceptable fits for all of the galaxies.

3.4. Spatial distribution

We next investigated the spatial distribution of the point-sources in a subset of the galaxies which contained sufficient sources. We created a set of radial bins centred on the X-ray centroid and each containing at least 15 sources. We compared the radial profiles of the sources with the optical light, which we modeled as a de Vaucouleurs profile, the effective radius of which was fixed to the appropriate K-band value determined from 2MASS (Jarrett 2000). We also included an additional, constant, component to account for interloper sources, which should be approximately uniformly sprinkled over the *Chandra* field. Fitting was performed with a Cash-C statistic minimization algorithm.

Since the effects of source detection incompleteness depend on the density of sources, the width of the point-

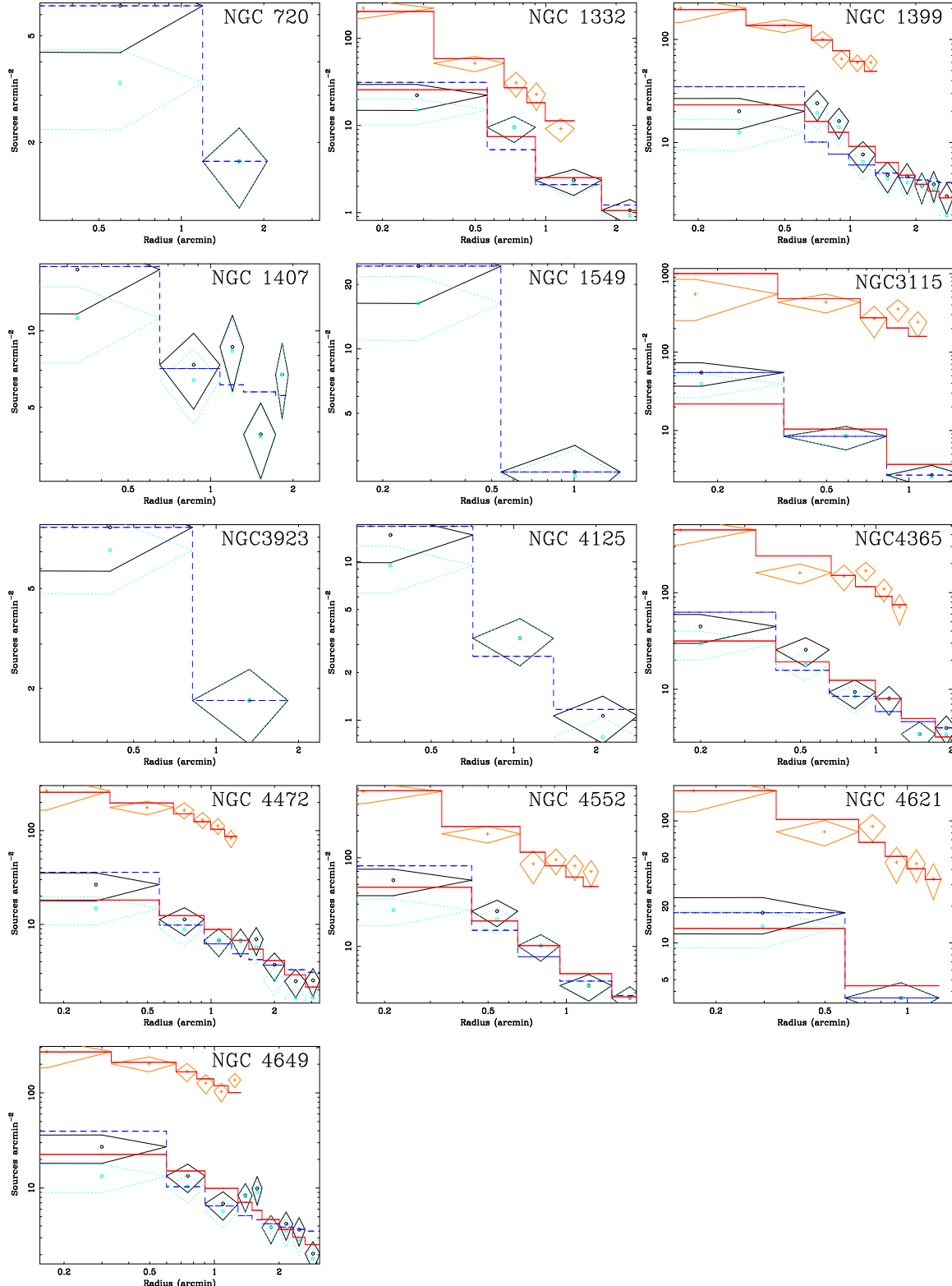


FIG. 3.— Spatial distribution of the LMXBs in those galaxies with sufficient sources. Shown are the data-points having corrected for spatial variation in source detection incompleteness (circles; black) and, where appropriate, the best-fitting model to a suitably weighted combination of the distributions of red and blue GCs (solid line; red). The distribution of the GCs, corrected for incompleteness, is also shown, with arbitrary scaling for clarity (crosses; orange) and the same best-fitting model. The dashed line (blue) shows the distribution of the optical light. For comparison, we also show the data-points having not corrected for the spatial variation in source incompleteness (triangles; light blue).

TABLE 2
LMXB SPATIAL DISTRIBUTION GOODNESS-OF-FIT

Galaxy	prob(light)	prob(GC,tot)	prob(GC,weight)
NGC720	0.35
NGC1332	0.10	0.15	0.090
NGC1399	1.0×10^{-3}	0.48	0.85
NGC1407	0.20
NGC1549	0.12
NGC3115	0.78	0.010	0.060
NGC3923	0.20
NGC4125	0.14
NGC4365	0.070	0.070	0.22
NGC4472	0.23	0.29	0.97
NGC4552	0.080	0.010	0.44
NGC4621	0.24	0.13	0.21
NGC4649	3.0×10^{-3}	0.32	0.44

NOTE. — The probability that the radial distribution of LMXBs is the same of the optical light (prob(light)) in each galaxy and the probability that it is the same as that of the GC population (prob(GC,tot)), or a weighted combination of the red and blue GC distributions (prob(GC,weight); *see text*).

spread function and the “background” count-rate (e.g. Kim & Fabbiano 2003), it varies spatially across the field of view. It was therefore necessary to take this into account when fitting the radial profile of sources. We discuss in general how we estimated the effects of source detection incompleteness on the XLF in § 4.1. We computed a similar correction appropriate for each radial bin, with which we weighted an assumed X-ray luminosity function (assumed to be the best-fitting broken powerlaw XLF we found in § 4.2) that was then integrated from $10^{37} - 2 \times 10^{39} \text{ erg s}^{-1}$ so as to estimate the fraction of sources detected as a function of radius.

In Fig 3 we show the spatial distribution of the point-sources in the subsample, both with a correction for the spatial variation in completeness applied, and with no correction. Outside the innermost 0.5' (in which incompleteness effects are most severe) the radial distribution of sources agrees very well with the optical light. Inside this region we find an excellent agreement between the source distribution and the optical light in approximately half of the tested galaxies. In the remaining galaxies, the optical light appears to over-predict the number of sources considerably. To determine the goodness-of-fit, we performed 100 Monte-Carlo simulations (increasing the number if the estimated goodness-of-fit was below 1%), where artificial data-sets were simulated from the best-fitting models and were fitted with the same model. The fraction of simulations with a larger Cash-C statistic (i.e. poorer fit) than for the real data was adopted as the null hypothesis probability (prob(light)), as shown in Table 2. If the LMXBs are, in general, distributed like the optical light, the distribution of prob(light) should, for these 13 galaxies, be uniform over the interval 0–1. Using a Kolmogorov-Smirnov (K-S) test (as implemented in Press et al. 1992), the probability the distributions are the same is only 2×10^{-5} . Considering only those galaxies for which we also have sufficient-quality GC data to measure the GC radial distribution as well (below), this probability is 0.05%.

If a substantial fraction of LMXBs are produced in GCs, we might expect the radial distributions of the two populations to be similar. Since the field of view of

the WFPC2 is significantly more restricted than *Chandra*, it was necessary to fit the LMXB and GC data with the same model simultaneously. To parameterize the GC distribution, we adopted a “beta” model ($\propto (1 + (R/R_c)^2)^{0.5-3\epsilon}$, where R_c and ϵ are parameters of the fit), and we additionally allowed a constant background component for the LMXBs (as discussed above). The data were of sufficient quality to enable this for 8 of the galaxies, and the null hypothesis probabilities are reported for this comparison in Table 2. We find moderately good agreement in most of the galaxies between the two distributions, although in two galaxies the null hypothesis probability was <5%. Blue GCs are known to have a considerably flatter distribution than their red counterparts (e.g. Paper II), while LMXBs are preferentially found in red GCs, and so a comparison with the radial distribution of the total GC population may not be entirely appropriate. We therefore also compared the radial distribution of the LMXBs to a weighted combination of the radial profiles of the red and blue GCs, taking into account the fraction of LMXBs expected to be produced in each population. For this model we found reasonably good agreement between the distributions in all of the galaxies. The null hypothesis probabilities for these fits are shown in Table 2. Based on a K-S test, as described above, we found that the distributions of these probabilities agrees with expectation (a uniform distribution) with a null hypothesis probability of 17%, significantly higher than the equivalent comparison with the optical light (0.05%).

4. X-RAY LUMINOSITY FUNCTIONS

4.1. *Source detection incompleteness*

In order to measure the point-source XLF it is extremely important to take into account the effects of source detection incompleteness and the Eddington bias, where the flux measurement errors distort the XLF shape (e.g. Kim & Fabbiano 2004). Kim & Fabbiano (2003) presented a possible strategy to correct the data for these effects. In order to maintain the statistical integrity of the data, we preferred to apply a correction to the model, and so adopted a modified strategy, which incorporates some aspects of the algorithm of Wang (2004).

For each galaxy, we performed a set of Monte-Carlo simulations, initially using 20 flux bins (corresponding approximately to equally-spaced bins from 1–20 detected counts), which entailed adding simulated sources to the image of each galaxy and then assessing the performance of the detection algorithm at finding and characterizing them. For many of the galaxies, we found that almost all of the sources expected to contain ~ 20 photons are detected, and so we assumed that any brighter sources will always be detected. In those galaxies for which this was not the case, we added additional simulations, logarithmically spaced in flux space, until $\sim 95\%$ completeness was achieved in any bin. In each flux bin, we performed 20 such Monte-Carlo simulations, in each of which we added 20 sources; adding them 20 at a time does not significantly increase source confusion since most galaxies had many more than 20 LMXBs in the total field of view. We assumed that the point-sources were distributed approximately as the optical light (§ 3.4). For each simulated source, to determine the number of photons to

TABLE 3
XLF FITTING RESULTS

Galaxy	N_{src}	f_{cover}	$L_{X,min}$ (10^{38} erg s $^{-1}$)	$L_{X,20}$ (10^{38} erg s $^{-1}$)	Prob	beta	L_X (10^{38} erg s $^{-1}$)	prob(H_0)	β_1	L_{break} (10^{38} erg s $^{-1}$)	β_2	L_X (10^{38} erg s $^{-1}$)
IC4296	11	0.41	8.1	20.	0.080	$2.9^{+1.5}_{-0.9}$	$8200^{+1400000}_{-7800}$	0.16	1.4	2.2	...	940^{+730}_{-520}
NGC720	22	0.37	1.0	4.8	0.050	2.1 ± 0.4	400^{+300}_{-170}	0.13	1.4	2.2	<2.2	280 ± 130
NGC1332	29	0.25	0.47	1.5	0.69	$2.4^{+0.5}_{-0.4}$	320 ± 150	0.49	1.4	2.2	...	240^{+90}_{-70}
NGC1387	10	0.38	0.96	1.9	0.50	3.5 ± 1.5	370^{+1700}_{-290}	0.060	1.4	2.2	...	$61^{+48.}_{-34.}$
NGC1399	144	0.57	0.22	0.91	0.11	2.2 ± 0.2	690 ± 110	< 0.01	1.4	2.2	$3.2^{+0.9}_{-0.6}$	540 ± 90
NGC1404	19	0.40	1.1	2.1	0.040	$2.3^{+0.5}_{-0.4}$	230 ± 190	0.61	1.4	2.2	>1.5	140^{+70}_{-50}
NGC1407	88	0.48	0.71	2.6	0.13	2.0 ± 0.2	630 ± 140	0.39	1.4	2.2	$2.3^{+0.6}_{-0.5}$	470^{+100}_{-90}
NGC1549	37	0.49	0.53	2.4	0.51	2.1 ± 0.3	160^{+60}_{-50}	0.51	1.4	2.2	>1.4	140^{+50}_{-40}
NGC1553	23	0.39	0.82	1.9	0.010	1.8 ± 0.4	100^{+60}_{-40}	0.26	1.4	2.2	...	$82^{+44.}_{-34.}$
NGC3115	44	0.37	0.091	0.36	0.13	1.7 ± 0.2	$79^{+53.}_{-36.}$	0.60	1.4	2.2	...	$66. \pm 23.$
NGC3585	31	0.53	0.38	1.7	0.20	$2.0^{+0.4}_{-0.3}$	110^{+50}_{-40}	0.47	1.4	2.2	...	$97. \pm 38.$
NGC3607	16	0.41	0.85	2.9	0.36	$3.5^{+1.4}_{-0.9}$	670^{+3900}_{-500}	0.030	1.4	2.2	...	$94^{+56.}_{-43.}$
NGC3923	30	0.51	0.83	4.4	0.56	$2.2^{+0.5}_{-0.4}$	240^{+200}_{-100}	0.49	1.4	2.2	...	150^{+70}_{-60}
NGC4125	31	0.45	0.47	1.3	0.040	$1.9^{+0.5}_{-0.4}$	$88^{+56.}_{-42.}$	0.19	1.4	2.2	<4.6	$74^{+41.}_{-33.}$
NGC4261	38	0.49	0.69	3.7	0.070	$2.7^{+0.5}_{-0.4}$	610^{+790}_{-280}	0.16	1.4	2.2	>1.7	240^{+90}_{-70}
NGC4365	104	0.53	0.30	1.4	0.37	2.0 ± 0.2	320^{+70}_{-60}	0.59	1.4	2.2	3.0 ± 1.6	290 ± 60
NGC4472	145	0.61	0.22	1.2	0.050	2.2 ± 0.2	470 ± 80	< 0.01	1.4	2.2	$3.0^{+1.2}_{-0.9}$	410 ± 70
NGC4494	13	0.46	0.82	2.6	0.60	$2.2^{+1.1}_{-0.6}$	$58^{+60.}_{-34.}$	0.91	1.4	2.2	...	$47^{+37.}_{-27.}$
NGC4552	79	0.49	0.13	0.61	0.13	1.8 ± 0.2	180^{+60}_{-50}	0.81	1.4	2.2	>0.74	160^{+40}_{-30}
NGC4621	34	0.49	0.45	1.6	0.24	$2.0^{+0.4}_{-0.3}$	$87^{+47.}_{-35.}$	0.70	1.4	2.2	<4.2	$80. \pm 37.$
NGC4649	121	0.59	0.25	1.4	0.13	2.1 ± 0.2	420^{+80}_{-70}	0.17	1.4	2.2	$2.7^{+1.0}_{-0.8}$	370^{+70}_{-60}
NGC5018	13	0.46	2.4	9.5	0.57	$2.3^{+1.5}_{-0.7}$	330^{+3500}_{-230}	0.73	1.4	2.2	>1.2	170 ± 140
NGC5846	16	0.45	1.7	3.5	0.22	$2.4^{+0.9}_{-0.6}$	240^{+920}_{-150}	0.47	1.4	2.2	>0.54	110^{+70}_{-50}
Composite	0.1	...		< 0.001	1.84 ± 0.05	1950 ± 140	0.03	$1.40^{+0.11}_{-0.13}$	$2.2^{+0.65}_{-0.56}$	$2.84^{+0.39}_{-0.30}$	1670 ± 130
GC	0.2	...	0.04	1.59 ± 0.16	413^{+128}_{-94}	0.64	1.4	2.2	2.84	248 ± 38
Field	0.1	...	< 0.01	1.89 ± 0.11	448^{+78}_{-69}	0.03	1.4	2.2	2.84	404 ± 55

NOTE. — The best-fitting parameters derived from fitting the XLF of each galaxy, and the composite XLFs of all the sources (“composite”). We also show fit results for the composite XLF of LMXBs in GCs (“GC”) and those in the field (“field”). Listed are the number of sources used in fitting the XLF (N_{src}), the fraction of the total galaxy light within the region in which the XLF is computed (f_{cover}), the approximate minimum L_X of sources contributing to the XLF ($L_{X,min}$), the approximate L_X of a source containing 20 photons ($L_{X,20}$), the null hypothesis probability (prob(H_0)), the differential logarithmic slope (β), and the integrated luminosity of the X-ray sources in the range $L_X=10^{37.2} \times 10^{39}$ erg s $^{-1}$ (see text). Fit results are also shown for a broken power law model. For individual galaxies, the slopes above and below the break (β_2 and β_1 , respectively) and the break luminosity, L_{break} , were fixed at values obtained for the composite XLF. For each galaxy, we list in the β_2^{free} column the value of this parameter if allowed to fit freely, when it could be constrained. Error bars are quoted at the 90% confidence limit. Where no error-bars are quoted on fit parameters, they were fixed at the given value.

simulate we computed a count-to-flux conversion by creating local ancillary spectral response files and an on-axis redistribution matrix and folding our preferred powerlaw spectral model through them. The point-source images were derived at each point by bilinear interpolation of the *Caldb* PSF images for a 1 keV point-source at various focal-plane positions, and finally Poisson noise was added.

In any arbitrary region of the *Chandra* field of view, for each flux bin this yielded the fraction of simulated sources which were detected and the *measured* count-rates (hence fluxes) of these sources. For brighter sources than those simulated, we assumed 100% completeness and that the distribution of measured fluxes is given by the Poisson statistics. Since the XLF comprises a histogram of the numbers of sources detected in a series of narrow flux bins, this information is sufficient to construct a “response matrix” through which any model to fit the XLF can be folded, analogous to X-ray spectral-fitting (e.g. Davis 2001) to take account of both incompleteness and the Eddington bias. We note that this method also applies the same correction to the interlop-

ers, which is formally incorrect since their spatial distribution is much flatter than the optical light. However, there were few interlopers in the regions of interest so this should not significantly affect our results.

4.2. XLF fitting

To measure the XLFs of the galaxies, we computed histograms of the measured numbers of sources as a function of flux. We considered only point-sources within D_{25} and excluded the innermost 20'' (where source detection may be uncertain; § 3.4). The data were regrouped to ensure at least 5 sources per bin, and the differential XLFs fitted using dedicated software which folded the model through the response described in § 4.1. To perform the fit we adopted the Cash-C statistic and parameter space was searched for a global minimum. To assess the goodness-of-fit, we adopted a Monte-Carlo strategy. Adopting the best-fitting model, we simulated 100 fake data-sets which were subsequently fitted. We adopted the fraction of simulations which yielded a best-fitting Cash statistic value higher (i.e. worse) than obtained for the real data as the null hypothesis (the model describes the data) probability (prob(H_0)). To account for interlopers, we adopted

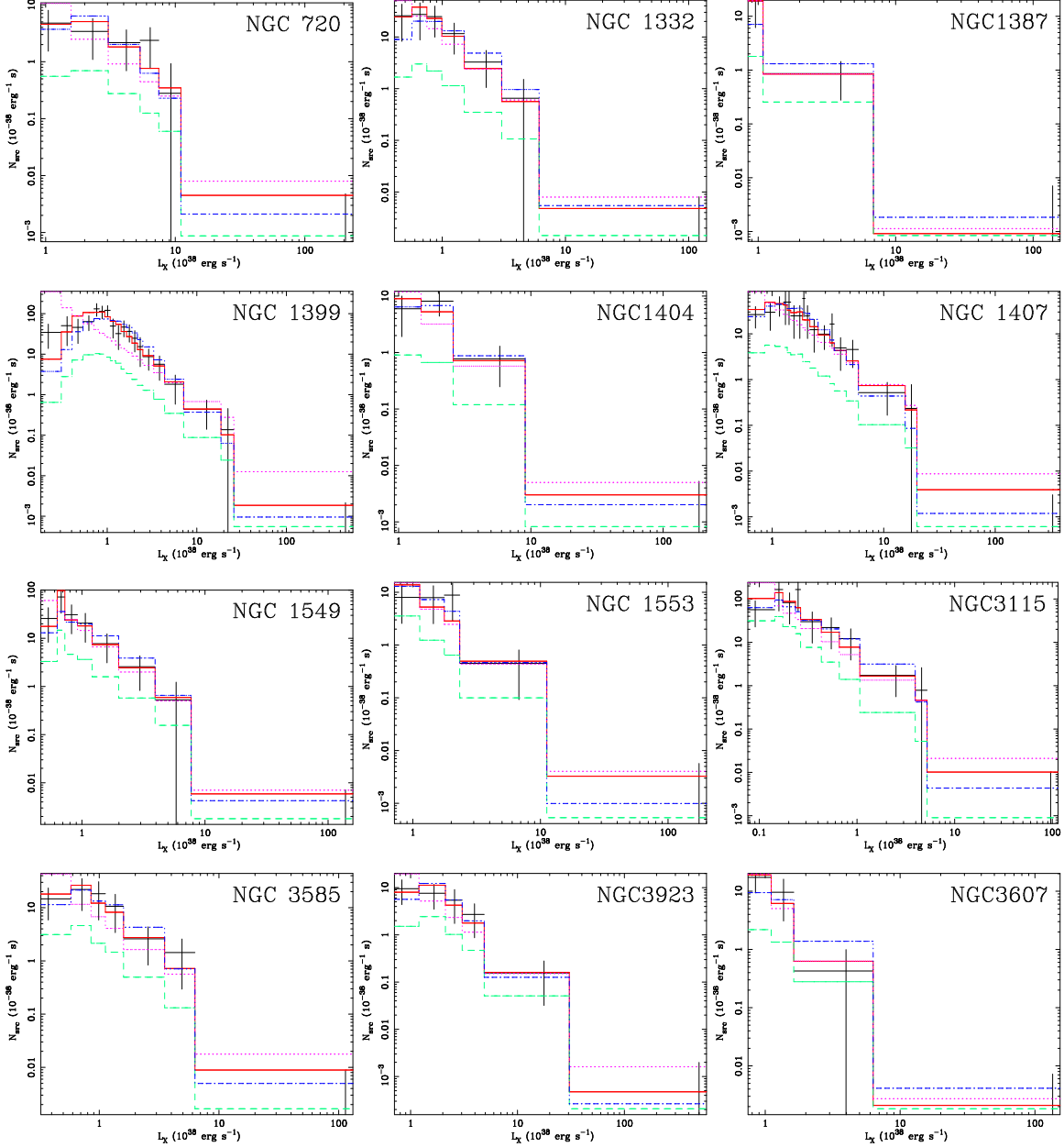


FIG. 4.— Individual differential XLFs for half of the galaxies (continued in Fig 5), shown with the best-fitting power law model (solid line; red), corrected for source detection incompleteness and the Eddington bias. The expected contribution from background AGN is shown as a dashed line (blue-green) as is the best-fit model to the composite XLF of all the galaxies (dash-dot-dot; blue). For comparison, the best-fit simple power law model, without incompleteness correction, is also shown (dotted line; magenta).

the hard-band XLF relation for sources in the Chandra Deep Field– South (Tozzi et al. 2001), correcting to the spectral-fitting band used in the present work, and the area of sky under scrutiny. Since the slope of the interloper XLF at high luminosities is similar to that of a typical early-type galaxy (Kim & Fabbiano 2004), it was not possible to fit the background normalization freely and so it was fixed. To investigate the sensitivity of our results to this assumption, we have experimented with the effect of varying the normalization by $\pm 50\%$. We found that this typically caused changes in the best-fitting parameters which were smaller than the statistical errors.

We found that we were generally able to fit the XLF of each galaxy adequately with a simple powerlaw model

of the form:

$$\frac{dN}{dL} \propto L^{-\beta} \quad (1)$$

The best-fitting results are shown in Table 3, and the XLFs are shown in Figs 4–5. In Table 3 we list the total luminosity in the range $10^{37}–2 \times 10^{39} \text{ erg s}^{-1}$ determined from our fit, having been corrected upwards by the fraction of optical light which falls outside the region in which the XLF was computed. This correction allowed us approximately to take account of the fact that not all the LMXBs are expected to lie in this region, since the spatial distribution of the LMXBs is generally close to that of the optical light. For NGC 5845 there were insufficient sources within the fitting region, and so we omit it from this table. For the 7 galaxies in our sample which over-

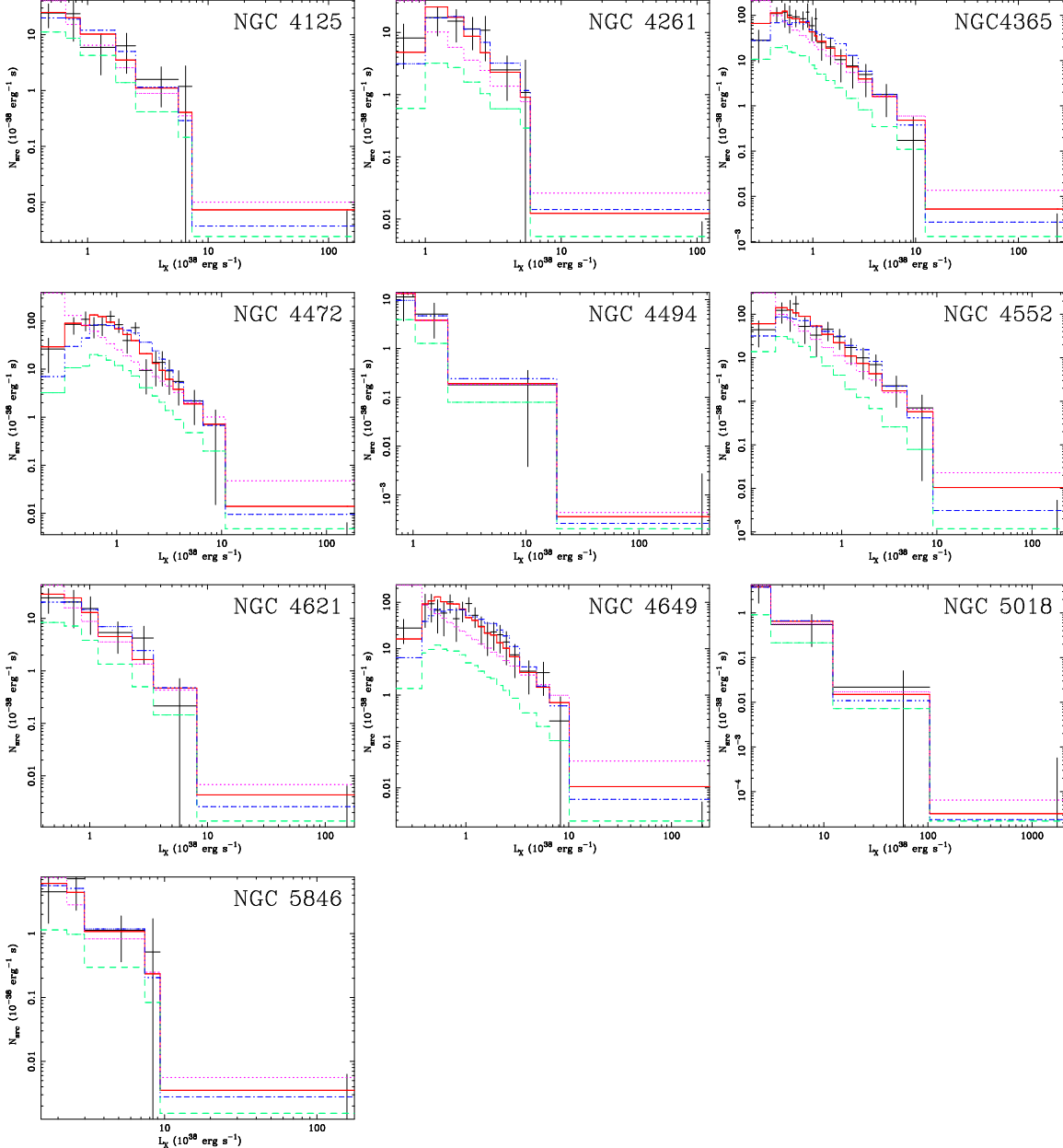


FIG. 5.— Same as Fig 4 for the remaining galaxies.

lapped that of Kim & Fabbiano (2004), we found good agreement, within the error-bars, between the measured values of β . Xu et al. (2005) obtained an incompleteness-corrected fit for NGC 4552, but found a slightly steeper β (~ 2.2) than we obtained. The reason for the discrepancy is unclear, although these authors fitted the cumulative luminosity function which is difficult to interpret due to correlations between adjacent data-points. Given that a single powerlaw model was typically an adequate fit, we found that we were generally unable to constrain the parameters of a broken powerlaw fit to the data.

There was remarkably little variation in β , indicating striking uniformity in the XLF shape of LMXBs in early-type galaxies. However, there is evidence of a small, but statistically-significant variation in slope. In Fig 6 we show how β varies as a function of the X-ray source detection completeness, f_i^X , defined as the fraction of actual

sources with $L_X = 10^{37} - 2 \times 10^{39}$ erg s $^{-1}$ which are detected. This is obtained by integrating the completeness-corrected and the uncorrected XLFs over the appropriate flux range. To prevent spurious correlations, we fixed $\beta = 2.0$ for this calculation. The data show a clear anti-correlation; using Spearman's rank-order correlation test, we found a probability of $\sim 7 \times 10^{-5}$ that the data are uncorrelated. This correlation indicates that the XLF, on average, must flatten at low L_X . If the “true” XLF is, in fact, a broken powerlaw which flattens below the break then the measured β will be an “average” of the slopes above and below it. As the data become more incomplete there are fewer sources below the break to weight the fit, so β asymptotes to the high- L_X slope. Since β , where the data are very complete, appears to asymptote to a value significantly flatter than 2.0, we conclude that β at low luminosities must, similarly, be

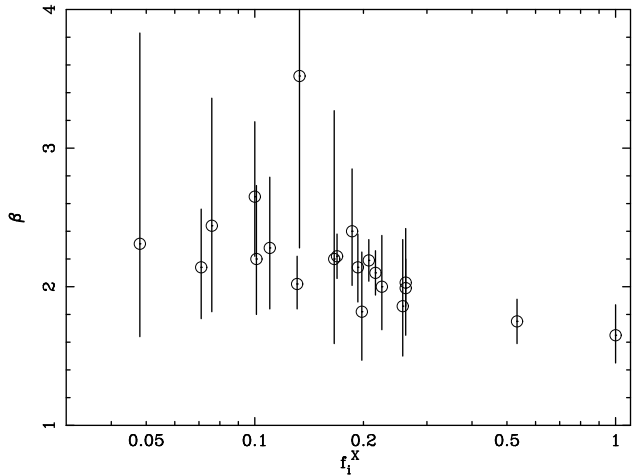


FIG. 6.— Plot of XLF slope, β as a function of source detection completeness, f_i^X . Note the correlation.

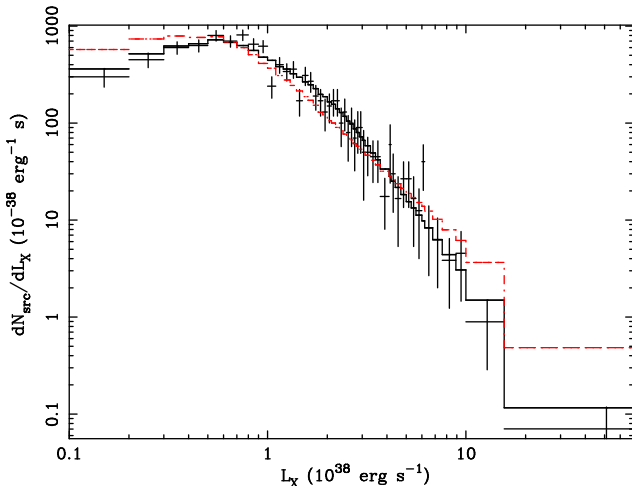


FIG. 7.— Composite XLF of all LMXBs, fitted with a simple power law (dashed line) and a broken power law (solid line). The models have been corrected for source detection incompleteness and the Eddington bias.

significantly less than 2.0. We note that, if we exclude the two most complete data-points from this comparison, we find that the probability of no correlation is still $\sim 2 \times 10^{-3}$, indicating that this result is not solely driven by these data.

4.3. Composite XLF

Given the trend for systematically flatter XLFs with increasing source detection completeness, we next experimented with adding the XLFs in order to improve S/N. We combined all detected sources for all of the galaxies into a single source list, and used that to generate the luminosity function data-points. To account for source detection incompleteness and the Eddington bias, we performed a weighted addition of the individual responses generated for each galaxy, using the number of observed sources as the weighting factors. We grouped the data identically to § 4.2, and similarly adopted the Cash-C fit-statistic.

We first fitted a single power law to the data, including a component to account for the expected background sources (estimated by adding the contributions antici-

pated for each galaxy). We found this model to be a very poor fit to the data (Fig 7). The best-fitting β (1.7) was much lower than we obtained for each galaxy individually. This is easily understood since this shallow slope is largely driven by the apparent paucity of sources at low L_X ($\lesssim 6 \times 10^{37} \text{ erg s}^{-1}$), consistent with the XLF flattening at low L_X . We next tried to fit the data with the truncated powerlaw model of Sivakoff et al. (2003), which gave a break at $6.7 \times 10^{38} \text{ erg s}^{-1}$ but failed to reproduce very well the shape of the XLF at low luminosities ($\text{prob}(H_0) < 0.1\%$). Finally, we fitted a broken powerlaw to the composite XLF. This gave a significantly better fit to the data; although the formal $\text{prob}(H_0)$ is only 3%, the deviations from a good fit are primarily due to individual discrepant data-points which are unlikely to bias the fit. The best-fitting parameters are shown in Table 3, and the best-fit model is shown in Fig 7.

We caution that, at the lowest luminosities the composite XLF is largely dominated by two galaxies, NGC 3115 and NGC 4552 and there exists a possibility that the XLFs of these two systems are not representative of the whole population of early-type galaxies. If that is the case, it may bias the shape we find for the composite low- L_X XLF. With our current data it is not possible entirely to rule out such a possibility; instead it must be tested using very deep *Chandra* observations of other galaxies. In the present work we take this fit at face value, but are careful to investigate the sensitivity of any derived quantities to the low- L_X slope.

To ensure that the broken power law fit did not arise as an artifact of our analysis, we experimented with simulating a simple power law XLF appropriate for each galaxy, with $\beta = 2.0$. Combining these identically to the real data, we found that a simple power law model gave a good fit to the data. Conversely, if we simulated simple power law XLFs but with β fixed to the best-fit value for each galaxy, the composite XLF was very poorly fitted by a simple power law, and instead a broken power law was required. However the implied break luminosity ($\sim 1.3 \times 10^{39} \text{ erg s}^{-1}$) was considerably higher than that of the composite XLF and the best-fit model for the real data was an extremely poor fit.

Since the response matrices we used to correct for the effects of incompleteness were generated by adding a *finite* number of artificial sources to each image, this introduces a statistical error into the matrix, which we have not explicitly taken into account in our analysis. In order to assess whether the magnitude of this effect can lead to significant errors in our measured XLF shape, we performed 100 Monte-Carlo simulations, in which all the “response matrices” were re-created, then combined and used to fit the existing data. In the interests of speed, we did not re-create the matrices from first principles (as described in § 4.1), but instead, for each luminosity bin of artificial sources which were added to the images, we drew 100 random numbers, which were distributed in the same manner as the *observed* luminosities in this bin (including the fraction of non-detections). Treating these random values as though they were the recovered luminosities of artificial point-sources added to the image, we constructed a new “fake” response matrix. Although this procedure assumes that the “real” matrix is formally correct, the differences in the faked matrices should ac-

curately indicate the magnitude of the statistical errors in that matrix. We re-fitted the composite XLF with appropriately added ‘faked’ responses for each Monte-Carlo simulation, and assessed the $1-\sigma$ scatter in the best-fitting parameters, indicating the level of this source of error. We found errors of ± 0.02 , $0.06 \times 10^{38} \text{ erg s}^{-1}$ and 0.02 for β_1 , L_{break} and β_2 , respectively, which are considerably smaller than the statistical errors reported in Table 3.

If the XLFs of all the galaxies in the sample are essentially the same, and it is simply the lack of counting statistics which have enabled us to fit single power law models to each dataset individually (§ 4.2), we would expect that the best-fit composite XLF model should also provide a good fit for each galaxy. We list in Table 3 the quality of fit for this model when applied to each galaxy in turn, and the best-fit models are shown in Figs 4–5. On a case-by-case basis, we find some systems which marginally seem inconsistent with having a break at $\sim 2 \times 10^{38} \text{ erg s}^{-1}$; for example NGC 1399. In contrast, the broken powerlaw model seems marginally preferred in some other systems, such as NGC 4552 and NGC 1404. However, in none of these cases is the data of sufficient quality to distinguish strongly between the two models. On average the powerlaw and broken powerlaw fits seem to fit the data comparably well. Nonetheless, if either model is ‘correct’, the $\text{prob}(H_0)$ values listed for that model in Table 3 should be distributed uniformly between 0 and 1. We therefore tested this hypothesis with a K-S test. For the simple powerlaw model, the probability that $\text{prob}(H_0)$ are distributed uniformly is 1%. In contrast, for the broken powerlaw model, this probability is a more acceptable 65%.

Throughout the rest of the paper, unless otherwise stated, we assume that the XLF of all galaxies is the same as our best-fitting model to the composite XLF, and extends down to $10^{37} \text{ erg s}^{-1}$. In practice, this means that all the ‘completeness-corrected’ results presented in § 5 refer only to LMXBs with $L_X > 10^{37} \text{ erg s}^{-1}$. Since the very low L_X XLF is dominated by only two galaxies, which could bias its shape if they are not representative, we also assess how our conclusions would be affected by adopting an XLF shape which is much steeper in that luminosity regime (specifically an unbroken powerlaw model with $\beta = 2.0$).

5. GLOBULAR CLUSTER ASSOCIATIONS

We discuss in Paper II our data-reduction and analysis of archival HST WFPC2 data for 19 of the galaxies in our sample. In that paper, we provide detailed lists of all globular cluster candidates we detected, and relevant photometry and various derived quantities, such as GC specific luminosity. A number of the galaxies do not have WFPC2 data available, and so, for consistency, we do not consider them here. We consider only WFPC2 data for simplicity of our analysis, despite the availability of superior ACS data for some of the galaxies. In practice, useful ACS data are available only for less than half of the sample, whereas most have WFPC2 data. Even with the relatively shallow WFPC2 data, we were able to detect, in most objects, more than 75% of the GC light, which is sufficient for our present purposes. We focus only on central-pointings with the WFPC2, although for some of the galaxies there are multiple HST pointings. We

adopt this procedure since the *Chandra* PSF rapidly degrades off-axis, making matching GCs and LMXBs more challenging, and possibly introducing a systematic bias between those objects with multiple pointings and those with only one.

Since the absolute astrometry of *Chandra* is not expected to be accurate at sub-arcsecond precision, in order to assess possible matches between LMXBs and GCs, we allowed a translation and a rotation transformation between the GC and LMXB source lists, which were adjusted to maximize the number of matches. For self-consistency, we assumed that any GC candidate lying within $0.5''$ of a *Chandra* source centroid (comparable to the on-axis PSF) was associated with it. If, based on this criterion, more than one GC matches an LMXB, or if more than one LMXB matches a GC, we match the pair with the closest centroids, although this only affects a small fraction of sources. Where both the optical and X-ray images of the galaxy had clearly-defined centroids, we constrained the transformation to ensure approximately the same matching precision between them as between GCs and LMXBs. This typically had little effect in galaxies with a large number of LMXB-GC matches, but was an important constraint in other systems. In order to assess the number of spurious matches obtained by this procedure, we randomly generated fake GC source lists, scattering them approximately as the optical light until the total number of objects in the WFPC2 FOV matched that which was observed. Using the procedures outlined above, we determined the number of these sources apparently associated with an LMXB, which was typically less than ~ 1 .

5.1. Composite spectra of GC sources

We next investigated potential spectral differences between LMXBs hosted by red and by blue GCs. Exactly analogous to the analysis in § 3.3, we obtained composite spectra for those LMXBs associated with red GCs and those associated with blue GCs. We defined any candidate GC with $V-I > 1.1$ as red, and those GCs with $V-I < 1.1$ as blue³. The spectra are shown in Fig 2 (along with the composite spectrum of all LMXBs in the galaxies). Both spectra were well-fitted by the best-fit models for the entire population (for the powerlaw models, we obtained $\chi^2/\text{dof} = 109/137$ and $100/99$ for the red and blue GCs, respectively. For the bremsstrahlung models χ^2/dof was $111/137$ and $102/99$). There was no evidence of a systematically harder spectrum or intrinsic absorption for the blue-GC sources, in conflict with the model of Maccarone et al. (2004). Fitting simultaneously the blue-GC and red-GC data with the same bremsstrahlung model but allowing N_{H} to vary freely we obtained $N_{\text{H}} < 3 \times 10^{20} \text{ cm}^{-2}$ for the blue-GC sources and $< 10^{20} \text{ cm}^{-2}$ for the red-GC sources. The larger upper limit for the blue-GC case in part reflects the poorer counting statistics but in both cases we can rule out intrinsic absorption of the order of 10^{21} cm^{-2} .

5.2. GC and non-GC XLF

³ The colour at which between red and blue GC sub-populations are separated varies from galaxy to galaxy, but we suspect the GC properties of LMXB hosts depend on the metallicity rather than the sub-population to which they belong, hence we use a fixed $V-I$ division for all galaxies

TABLE 4
LMXB-GC PROPERTIES

Name	L_V^{FOV} ($10^{10} L_\odot$)	N_{GC} red blue	L_{GC}^{TOT} ($10^7 L_\odot$)	f_i^{GC}	$N_{X,obs}$	N_X	f_i^X	$N_{GC,X}$ red blue	N_{false}
NGC1332,	2.0 ± 0.5	65 133	8.3 ± 1.2	0.60	27	$86. \pm 19.$	0.29	3 3	0.70
NGC1387,	1.2 ± 0.2	28	0.79 ± 0.51	0.22	10	$26. \pm 10.0$	0.32	0	0.0
NGC1399,	2.0 ± 1.1	162 329	$12. \pm 1.$	0.81	42	160 ± 30	0.27	7 13	1.5
NGC1404,	1.7 ± 1.1	47 116	5.3 ± 0.9	0.74	11	$58. \pm 17.$	0.19	0 5	0.20
NGC1553,	2.7 ± 0.3	21 50	2.1 ± 0.5	0.76	13	$23. \pm 8.$	0.48	0 2	0.20
NGC3115,	1.08 ± 0.08	39 93	2.3 ± 0.4	0.92	33	$31. \pm 6.$	0.91	7 2	0.60
NGC3585,	3.0 ± 0.5	35 67	2.4 ± 0.4	0.83	21	$40. \pm 10.$	0.45	3 0	0.30
NGC3607,	2.4 ± 0.5	21 85	4.9 ± 0.9	0.62	19	$58. \pm 15.$	0.30	1 3	0.40
NGC4125,	3.2 ± 0.5	77 118	2.6 ± 0.4	0.74	23	$38. \pm 9.$	0.50	1 1	0.80
NGC4261,	3.4 ± 2.0	70 170	$11. \pm 1.$	0.56	17	$78. \pm 18.$	0.20	1 3	0.20
NGC4365,	2.3 ± 0.4	90 200	8.2 ± 0.9	0.81	42	$71. \pm 12.$	0.53	6 9	1.6
NGC4472,	3.9 ± 0.3	183 214	7.1 ± 0.7	0.83	37	$82. \pm 14.$	0.43	7 6	0.70
NGC4494,	1.5 ± 0.3	42 133	3.0 ± 0.4	0.86	8	$19. \pm 7.$	0.39	4 0	1.6
NGC4552,	1.3 ± 0.2	77 162	4.2 ± 0.5	0.85	36	$56. \pm 10.$	0.56	5 6	1.3
NGC4621,	1.7 ± 0.3	57 114	3.9 ± 0.5	0.86	27	$44. \pm 9.$	0.53	2 8	0.80
NGC4649,	2.9 ± 0.3	130 192	7.2 ± 0.7	0.87	35	$91. \pm 15.$	0.38	13 4	1.2
NGC5018,	9.7 ± 2.5	10 80	7.8 ± 1.8	0.47	8	$49. \pm 28.$	0.095	0 1	0.20
NGC5845,	1.9 ± 0.7	18 39	1.4 ± 0.8	0.47	2	$0.32 \pm 3.9.$	0.20	0 0	0.0
NGC5846,	2.6 ± 0.7	112 175	5.3 ± 0.6	0.76	8	$37. \pm 14.$	0.19	2 1	0.40

NOTE. — Details of the GC populations within the WFPC2 field of view. We show the total V-band luminosity in the field of view (L_V^{TOT}), the number of GCs (N_{GC}), divided into red and blue GCs (except for NGC1387, for which we do not have colour information; Paper II), the total GC luminosity (L_{GC}^{TOT}), corrected for incompleteness, the GC source detection completeness, f_i^{GC} , which is the fraction of the total GC luminosity detected. We also list the number of LMXBs observed in the WFPC2 field of view ($N_{X,obs}$), the (incompleteness-corrected) number of such sources in the WFPC2 field of view (N_X), the fraction of the LMXBs which are detected (f_i^X ; this is derived from our fits, not strictly from taking $N_{X,obs}/N_X$, which is more affected by statistical noise), the number of LMXBs with corresponding GC counterparts ($N_{GC,X}$) and the number of probable false GC-LMXB matches (N_{false}).

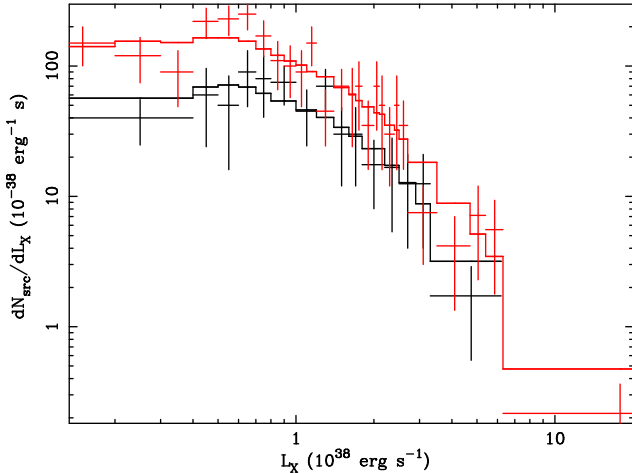


FIG. 8.— Composite XLFs of GC LMXBs (black) and field LMXBs (red), fitted with the best-fitting model for the entire LMXB population.

We accumulated composite XLFs of those LMXBs associated with GC and those which are in the WFPC2 field but not identified with a GC, exactly as described in § 4.3. In practice, we omitted any sources found in the very central regions of most of the galaxies (as discussed in Paper II), since features in the optical images, such as dust lanes, can give rise to false or ambiguous GC detections. In practice, this involved excluding regions of radius between $2''$ and $8''$. The XLFs were remarkably

similar in shape and both closely resembled the composite XLF for the entire source population (which was computed in a slightly different region). We therefore tried fitting both data-sets with the preferred broken powerlaw model fitted in § 4.3. Since the likelihood of an interloper being spuriously matched to a GC candidate is low, we assumed that all of the expected interloper sources only contributed to the non-GC XLF. The broken powerlaw model fitted both data-sets adequately (Table 3), indicating that the XLF of sources in GCs and those in the field are essentially the same.

5.3. Spatial distribution of GCs and LMXBs

We showed in § 3.4 that the spatial distribution of LMXBs closely follows that of red GCs (and also resembles the optical light outside the innermost $\sim 0.5'$) in a subset of galaxies in the sample. If some of the LMXBs observed in the field are born *in situ*, there may, nevertheless, be detectable differences between the radial distributions of field and GC LMXBs. Ideally we would like to address whether the spatial distributions of LMXBs in GCs resembles that of the GC population, while for field LMXBs it more closely resembles the optical light. However, given the limited radial range over which we have measured the GC spatial distribution, and the relatively small numbers of sources (both GCs and, in particular, LMXBs) that are detected, this is impractical. Therefore, we instead first tested, on a galaxy-by-galaxy basis and within the WFPC2 field of view, whether the

TABLE 5
DERIVED LMXB-GC PROPERTIES

Galaxy	S_L	$S_{N,X}$	$p_{GC,X}$	LMXB GC fraction			
		corrected	raw	corrected	raw	corrected	raw
NGC1332	0.42 ± 0.19	0.38 ± 0.08	0.11 ± 0.03	$0.018^{+0.012}_{-0.008}$	0.027 ± 0.018	$0.35^{+0.24}_{-0.16}$	$0.20^{+0.13}_{-0.09}$
NGC1387	0.065 ± 0.045	0.18 ± 0.07	0.071 ± 0.030	<0.18	<0.05	<1.0	<0.19
NGC1399	0.59 ± 0.53	0.65 ± 0.11	0.17 ± 0.03	$0.039^{+0.012}_{-0.009}$	$0.038^{+0.011}_{-0.009}$	0.55 ± 0.16	0.43 ± 0.13
NGC1404	0.32 ± 0.35	0.30 ± 0.09	0.061 ± 0.023	$0.037^{+0.026}_{-0.017}$	$0.029^{+0.021}_{-0.013}$	$0.58^{+0.41}_{-0.27}$	$0.40^{+0.28}_{-0.18}$
NGC1553	0.077 ± 0.024	0.071 ± 0.024	0.040 ± 0.015	$0.013^{+0.019}_{-0.009}$	$0.025^{+0.037}_{-0.019}$	$0.22^{+0.32}_{-0.16}$	$0.14^{+0.20}_{-0.10}$
NGC3115	0.21 ± 0.04	0.24 ± 0.04	0.27 ± 0.05	$0.026^{+0.013}_{-0.009}$	$0.064^{+0.031}_{-0.022}$	0.33 ± 0.16	$0.25^{+0.12}_{-0.09}$
NGC3585	0.081 ± 0.026	0.12 ± 0.03	0.060 ± 0.016	$0.015^{+0.016}_{-0.009}$	$0.026^{+0.029}_{-0.016}$	0.18 ± 0.19	$0.13^{+0.14}_{-0.08}$
NGC3607	0.20 ± 0.07	0.20 ± 0.05	0.066 ± 0.019	$0.026^{+0.023}_{-0.014}$	$0.034^{+0.030}_{-0.018}$	$0.33^{+0.29}_{-0.18}$	0.19 ± 0.17
NGC4125	0.082 ± 0.023	0.10 ± 0.02	0.062 ± 0.016	<0.015	<0.020	<0.27	<0.16
NGC4261	0.34 ± 0.34	0.20 ± 0.05	0.042 ± 0.013	$0.015^{+0.012}_{-0.007}$	$0.016^{+0.013}_{-0.008}$	$0.42^{+0.35}_{-0.22}$	0.22 ± 0.19
NGC4365	0.36 ± 0.11	0.27 ± 0.05	0.16 ± 0.03	$0.020^{+0.007}_{-0.006}$	0.046 ± 0.017	0.44 ± 0.16	$0.31^{+0.12}_{-0.09}$
NGC4472	0.18 ± 0.03	0.18 ± 0.03	0.082 ± 0.016	$0.019^{+0.007}_{-0.006}$	$0.031^{+0.012}_{-0.009}$	0.42 ± 0.16	$0.32^{+0.12}_{-0.09}$
NGC4494	0.20 ± 0.07	0.11 ± 0.04	0.037 ± 0.023	0.014 ± 0.019	0.014 ± 0.018	$0.37^{+0.50}_{-0.30}$	$0.30^{+0.40}_{-0.24}$
NGC4552	0.32 ± 0.10	0.37 ± 0.06	0.23 ± 0.05	$0.024^{+0.011}_{-0.008}$	0.040 ± 0.018	0.36 ± 0.17	$0.27^{+0.12}_{-0.09}$
NGC4621	0.23 ± 0.07	0.22 ± 0.05	0.14 ± 0.03	$0.026^{+0.012}_{-0.009}$	$0.053^{+0.025}_{-0.018}$	$0.46^{+0.22}_{-0.16}$	0.33 ± 0.15
NGC4649	0.25 ± 0.04	0.27 ± 0.04	0.098 ± 0.020	$0.031^{+0.010}_{-0.008}$	0.049 ± 0.016	0.53 ± 0.17	0.45 ± 0.15
NGC5018	0.080 ± 0.038	0.043 ± 0.025	$(6.9 \pm 3.4) \times 10^{-3}$	<0.073	<0.035	<1.4	<0.39
NGC5845	0.077 ± 0.062	$(1.5 \pm 18.) \times 10^{-3}$	$(9.2 \pm 12.) \times 10^{-3}$	<0.060	<0.033	$<62.$	<0.93
NGC5846	0.21 ± 0.09	0.12 ± 0.05	0.025 ± 0.013	0.016 ± 0.018	$(9.0^{+10.}_{-5.8}) \times 10^{-3}$	$0.50^{+0.56}_{-0.32}$	$0.32^{+0.37}_{-0.21}$

NOTE. — Derived properties for the LMXB and GC populations of the galaxies. We list the GC specific luminosity, S_L (Paper II) and the specific frequency of LMXBs ($S_{N,X}$). We also include the probability that a given GC has an LMXB counterpart ($p_{GC,X}$), and the fraction of LMXBs with a GC counterpart (LMXB GC fraction). For $S_{N,X}$, $p_{GC,X}$ and the fraction of LMXBs in GCs, we list the value corrected for incompleteness and GC colour effects (“corrected”) and a value derived directly from the data without any such correction. We stress that $p_{GC,X}$ and the LMXB GC fraction are *not* directly fitted in our analysis, but we provide them here for convenience in interpreting Figs 11 and 13. The error-bars for $S_{N,X}$, $p_{GC,X}$ and LMXB GC fraction are $1-\sigma$.

radial distances of the GC and field LMXBs from the galaxy centre are consistent with being drawn from the same distribution. We assessed this with a Kolmogorov-Smirnov test and only considered galaxies with at least 3 GC-LMXB matches. In all cases the hypothesis that the two samples were the same could not be rejected at the 5% significance level or better. Next, we applied the same test to the entire population of LMXBs in the WFPC2 field, and similarly found a null hypothesis probability of $\sim 64\%$, indicating excellent agreement between the two distributions.

5.4. Probability that a GC contains an LMXB

The probability that a GC is associated with an LMXB does not depend on the LMXB luminosity, as indicated by the similarities in the XLF of the GC and non-GC X-ray sources. Although in Paper II we compute the mass and metallicity of each GC, in order to investigate how the presence of an LMXB depends upon the GC properties, we focus only on the luminosity and colour. We adopt this approach for two reasons. Firstly, the metallicity errors are typically fairly large, and a non-negligible fraction of them have metallicities which peg at the maximum or minimum values allowed in our conversion. Secondly, as we show in Paper II, the colour and luminosity of the GC populations are independent of each other, making this analysis simpler. Since our optical data comprised, at most, 2 colours, we were not able to break the age-metallicity degeneracy and so we assumed that all colour dependency reflects a metallicity effect (c.f. Kundu et al. 2003). For consistency with past work, we make the conversion between colour and metallicity by using the relation of Kundu & Whitmore (1998), $\log(Z_{Fe,GC}) = -5.89 + 4.72(V - I)$. To investi-

gate how the probability that a GC contains an active LMXB, $P(GC,X)$, depends upon the properties of the GC, we adopted the hypothesis:

$$P(GC,X) = p_{GC-X} \left(\frac{L_{GC}}{L_0} \right)^\alpha \left(\frac{Z_{GC}}{Z_0} \right)^\gamma \quad (2)$$

where L_{GC} is the V-band luminosity of a GC, Z_{GC} is its metallicity, L_0 is the luminosity of the turnover in the globular cluster luminosity function (GCLF) for the entire GC population ($\sim 7.2 \times 10^4 L_\odot$), and Z_0 is the metallicity corresponding to the peak of the GC colour distribution ($\sim 0.08 Z_\odot$; Paper II). The indices α and γ , and the normalizing constant, p_{GC-X} , are to be determined by the data.

5.4.1. Globular Cluster luminosity functions

Considering only those GC hosting an LMXB, we computed a globular cluster luminosity function (GCLF), to compare with that of the entire population (Paper II). We discuss in Paper II how the composite V-band GCLF is accumulated and how we fitted the data to account for source detection incompleteness. We assumed that the detection incompleteness of GCs hosting LMXBs in any galaxy depends upon luminosity in the same way as that of the whole GC population. For simplicity, we omitted NGC 1399 and NGC 1404 from this calculation, since they did not have any V-band photometry. We fitted the composite GCLF using a maximum-likelihood fitting algorithm and minimizing the Cash-C statistic exactly as described in Paper II. We found the GCLF of the X-ray luminous source population could be fitted by a single

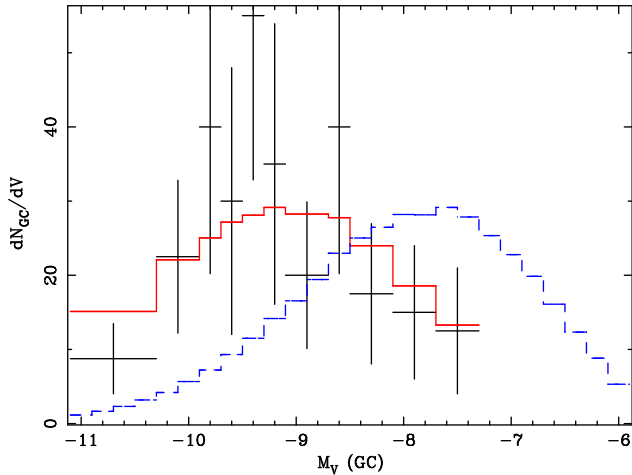


FIG. 9.— Composite globular cluster luminosity functions of all GCs associated with an LMXB. The best-fit Gaussian model is shown (solid line), along with the best-fit model to the GCLF of the entire population, rescaled for clarity (dashed line). The models have been corrected for source detection incompleteness.

Gaussian distribution, i.e.

$$\frac{dn_{GC}}{dV} = \frac{N_{GC}}{\sqrt{2\pi}\sigma} \exp\left(-\frac{(V - V_T)^2}{2\sigma^2}\right) \quad (3)$$

where n_{GC} is the number density of GCs, as a function of V-band luminosity (V), N_{GC} is the total number of GCs and V_T is the apparent V-band peak luminosity (“GCLF turnover”). Based on 100 Monte-Carlo simulations, we estimated $\text{prob}(H_0) = 46\%$. We found $\sigma = 1.0^{+0.4}_{-0.2}$, in agreement with that of the entire population (~ 1.5), but the absolute magnitude of the V-band turnover was $-9.0^{+0.3}_{-0.2}$, approximately 2.0 magnitudes brighter than the global GCLF, consistent with previous observations (Kim et al. 2006b). Fig 9 shows the GCLF, along with the best-fitting Gaussian distribution and, for comparison purposes, the best-fit Gaussian for the entire GC population, suitably rescaled.

Since there is no correlation between L_{GC} and Z_{GC} (Paper II; § 5.4.2), the dependence of $P(GC, X)$ on these quantities can be assessed independently by considering separately the GCLF and the GC colour distributions. It follows from Eq 2 that the GCLF of X-ray hosting GCs will have the same shape as the entire population, but be systematically shifted by $-0.92\alpha\sigma^2$ magnitudes. This implies that $\alpha = 1.01 \pm 0.19$.

5.4.2. Globular Cluster colour distributions

We constructed histograms of the numbers of GC as a function of V-I, each bin having a width of 0.05 mag. The histogram could be adequately fitted (*via* a Cash-C minimization algorithm) with a single Gaussian model, i.e.

$$\frac{dn_{GC}}{d(V - I)} = \frac{N_{GC}}{\sqrt{2\pi}\sigma_c} \exp\left(-\frac{((V - I) - (V - I)_0)^2}{2\sigma_c^2}\right) \quad (4)$$

where n_{GC} is the number density of GCs, as a function of V-I colour, N_{GC} is the total number of GCs and $(V - I)_0$ is the mean of the colour distribution. We found $(V - I)_0 = 1.08 \pm 0.02$ mag and $\sigma_c = 0.14 \pm 0.2$ mag. This distribution is significantly redder and narrower than the

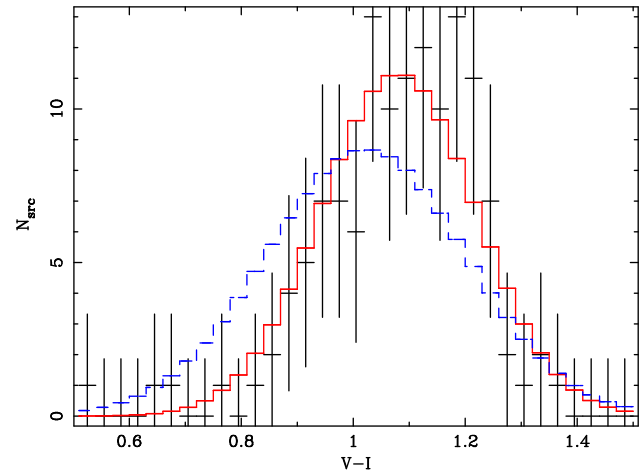


FIG. 10.— Composite colour distribution histogram of all GCs associated with an LMXB. Also shown are the best-fit Gaussian model (solid line; red) and the best-fit Gaussian model for the entire GC population, suitably renormalized (dashed line; blue).

GC population as a whole (Fig 10; Paper II), implying the ratio of the probability that a red GC hosts an LMXB to the probability that a blue GC does is ~ 2 . We note that fitting these data with a simple Gaussian model is overly-simplistic since early-type galaxies generally exhibit bimodal GC colour distributions. However, the peaks of the metal-rich and metal-poor subpopulations are not cleanly separated in V-I space, and so the average colour distributions of the clusters in a galaxy can be parameterized by a simple Gaussian, which is sufficiently accurate for our present purposes.

The difference in σ between the population of GCs as a whole and the subpopulation hosting LMXBs is easily understood in terms of the statistical errors on the photometry, since luminous GCs preferentially host LMXBs. If we considered only those GCs with absolute V-band magnitude <-9.0 , we found $\sigma = 0.14$, in good agreement with the colour distributions of the LMXB hosts. The fainter GCs will have increasing statistical errors on their photometry, which will increase σ . Assuming no correlation between the colour and magnitude of a GC (Paper II), it is trivial to show from Eq 2 and our adopted colour-metallicity relation that the colour distribution of GCs hosting LMXBs should have the same shape as that of the entire population, but be shifted by $10.87\sigma^2\gamma$ magnitudes, implying $\gamma = 0.33 \pm 0.11$.

5.4.3. Probability that a GC hosts an LMXB

Given the shapes of the GCLFs and GC colour distributions for our sample (for our purposes the latter can be approximated as a Gaussian with a peak shifted by Δ_c magnitudes from that of the entire sample, and with width σ_c), it follows from Eq 2 that

$$N_{GC,X} - N_{false} = p_{GC-X} \frac{L_{GC}^{TOT}}{L_0} f_i^X f_i^{GC} \times \exp(59.0\gamma^2\sigma_c^2 + 10.9\gamma\Delta_c) \quad (5)$$

where $N_{GC,X}$ is the number of GC-LMXB matches, N_{false} the number of expected false matches, L_{GC}^{TOT} the total luminosity of GCs, L_0 the peak luminosity of the composite GCLF of the entire sample, f_i^X is the fraction of LMXBs which are detected and f_i^{GC} is the fraction

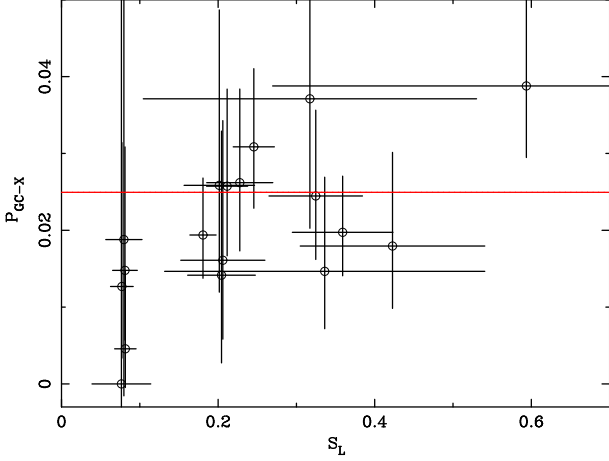


FIG. 11.— Incompleteness, colour and luminosity corrected fraction of GCs which contain an LMXB (see Eq 2), shown as a function of S_L . We also show the best-fitting model.

of the GC luminosity which is detected. For simplicity we here assumed that $\alpha = 1$, with which our data are consistent. For NGC 1387 we had no colour information for the GCs, and so we adopted $\Delta_c = 0.0$ and $\sigma_c = 0.14$.

Using the information in Tables 4 and 5, for any given value of p_{GC-X} Eq 5 gives the number of expected GC-LMXB matches. Matching this model to the observed numbers of sources *via* the Cash-C statistic, and adopting a maximum-likelihood fitting procedure similar to that outlined in § 4.2 we were able to place constraints on p_{GC-X} . We obtained a good fit to the data (prob(H_0)=63%) with $p_{GC-X}=0.025 \pm 0.004$. Integrating Eq 2 over the mean colour and luminosity distributions for the GC populations, this corresponds to a probability of 6.5% that a randomly chosen GC contains an LMXB with $L_X > 10^{37}$ erg s $^{-1}$. We show in Fig 11 p_{GC-X} computed directly from Eqn 5 for each dataset and the best-fit model value, as a function of GC specific luminosity, S_L . For comparison, if we replaced f_i^X with the equivalent value appropriate for a power-law XLF, assuming $\beta = 2.0$, we also obtained an acceptable fit (prob(H_0)=29%) with $p_{GC-X}=0.054 \pm 0.009$ (implying 14% of GC contain an LMXB with $L_X > 10^{37}$ erg s $^{-1}$).

5.5. Are any LMXBs formed in the field?

In order to test whether any LMXBs are formed in the field, we first adopted the simple hypothesis that:

$$N_X = \mu \frac{L_{GC}^{TOT}}{10^6 L_\odot} + \nu \left(\frac{L_V}{10^{10} L_{V\odot}} \right) \quad (6)$$

where N_X is the total number of LMXBs (corrected for source detection incompleteness), L_{GC}^{TOT} is the total luminosity of the GC and L_V is the V-band luminosity. We performed this comparison only within the WFPC2 FOV. For most of the galaxies in our sample, we tabulate in Paper II the specific luminosity of globular clusters, defined as $S_L=100L_{GC}/L_V$. From Eq 6, μ and ν can be trivially obtained from a plot of S_L versus the specific frequency of LMXBs, $S_{N,X}$, defined as $S_{N,X}=8.55 \times 10^7 N_X / (L_V / L_{V\odot})$ (assuming the absolute V-band magnitude of the Sun is 4.83: Maraston 1998). This is similar to the method adopted by Irwin (2005).

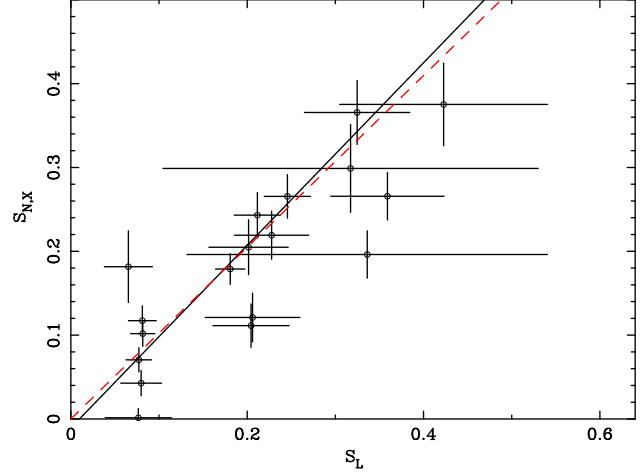


FIG. 12.— V-band specific frequency of LMXBs ($S_{N,X}$) *versus* specific luminosity of GCs (S_L) for the WFPC2 FOV. The best-fit straight-line relation is shown (solid line), along with the best-fit line if the intercept is fixed at 0 (dashed line; red)

Adopting our preferred broken powerlaw XLF to compute N_X (Table 5), we show in Fig 12 $S_{N,X}$ *versus* S_L . Taking account of errors on both x and y axes with a strategy similar to that outlined in Press et al. (1992), we fitted a straight line through the data. Initially fixing $\nu=0.0$, i.e. requiring that all LMXBs form in GCs, we found a reasonable fit, ($\chi^2/\text{dof}=23.1/18$) with $\mu = 1.20 \pm 0.12$. Allowing ν to fit freely, we found that the fit did not significantly improve ($\chi^2/\text{dof}=22.7/17$) and we constrained $\mu = 1.27^{+0.28}_{-0.22}$ and $\nu < 1.8$.

For a typical galaxy with $S_L \sim 0.2$, this implies that at most only $\sim 8\%$ of the LMXBs could be formed in the field. Since NGC 5845 is something of an outlier, being the smallest galaxy in our sample, we have investigated whether the results of our fit are biased by including this galaxy. Excluding this galaxy, we obtained similar results ($\chi^2/\text{dof}=19.4/16$, $\mu = 1.18^{+0.28}_{-0.21}$ and $\nu < 3.4$), implying it does not bias the fit. For comparison purposes, if we instead adopted a simple powerlaw XLF, with $\beta = 2.0$, we obtained a relatively poor fit for the case $\nu = 0.0$ ($\chi^2/\text{dof}=39/18$) with $\mu = 2.80^{+0.32}_{-0.28}$. Allowing ν to vary freely, the fit was similarly poor ($\chi^2/\text{dof}=38/17$) and we constrained $\mu = 3.07^{+0.76}_{-0.56}$ and $\nu \leq 3.6$.

5.6. GC LMXB retention fraction

The probability that an X-ray binary born in a GC is retained by the GC, correcting for incompleteness, $P(X,GC)$, is given by the relation:

$$N_{GC,X} - N_{false} = P(X,GC) \left(N_X - \nu \frac{L_V}{10^{10} L_{V\odot}} \right) f_i^X f_i^{GC} \quad (7)$$

We estimated both $P(X,GC)$ and ν by matching this model to the observed distribution of $N_{GC,X}$ *via* a fitting procedure similar to that described in §5.4.3. Initially we tested the hypothesis $\nu = 0.0$, i.e. all LMXBs form in GCs. We found that the data were well-fitted (prob(H_0)=81%), and we constrained $P(X,GC)=0.40 \pm 0.06$. Allowing ν to vary freely also gave a good fit (prob(H_0)=95%) with $P(X,GC)=0.53^{+0.11}_{-0.14}$ and $\nu = 6.3^{+1.7}_{-5.4}$, in agreement with our results in § 5.5. Fig 13

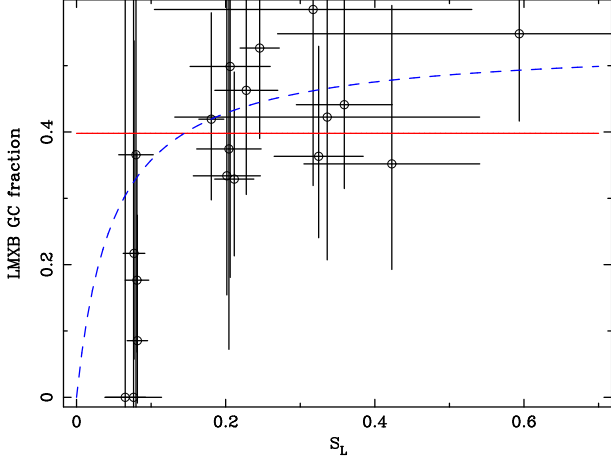


FIG. 13.— Incompleteness-corrected fraction of LMXBs associated with a GC, as a function of S_L . Shown are the preferred relations for the case where all sources form in GCs (solid line; red) and where LMXB formation in the field is proportional to the V-band luminosity (dashed line; blue).

shows values of $P(X, \text{GC})$ computed directly from the data (assuming all sources form in GCs), and the best-fit models. For comparison, if we adopted values of N_X and f_i^X appropriate for a single powerlaw XLF (with $\beta = 2.0$), we constrained $P(X, \text{GC}) = 0.55^{+0.12}_{-0.14}$ and $\nu = 15.1^{+3.9}_{-11.5}$.

6. DISCUSSION

6.1. The X-ray luminosity function

6.1.1. The shape of the XLF

When corrected for source detection incompleteness, we found that the XLF of early-type galaxies is very uniform in shape from object to object. We found that a simple powerlaw fit to the XLF of each galaxy was formally acceptable, but the slope of the model correlated with the source detection incompleteness, implying that the slope flattens at low L_X . Fitting the composite XLF we found that it is best modeled as a broken powerlaw, with a break at $(2.21^{+0.65}_{-0.56}) \times 10^{38} \text{ erg s}^{-1}$, and negative differential logarithmic slopes $1.40^{+0.10}_{-0.13}$ below the break and $2.84^{+0.39}_{-0.30}$ above. Still, a single powerlaw model with slope, $\beta \simeq 2.0$ was able to fit the XLF of each individual galaxy formally about as well at this model. A similar result was found by Kim & Fabbiano (2004) for a smaller sample of galaxies.

In Fig 14 we compare our best-fitting XLF, in cumulative form, with XLFs reported in the literature by a number of different authors. Considering the ranges for which each XLF has been found to be valid, we find excellent agreement between our best-fitting functional form and those reported in the literature, even that reported for Milky Way LMXBs by Grimm et al. (2002). We note that the absolute normalization of any of these models (except that of Grimm et al.) is arbitrary. Despite this good agreement it is still possible that the XLF we measure is biased at low luminosities, where the data were dominated by only two galaxies, NGC 3115 and NGC 4552, which may not be completely representative. Unfortunately, this cannot be ruled out with our current data, but will require deep XLFs measured for other early-type galaxies to assess it. Nonetheless, most

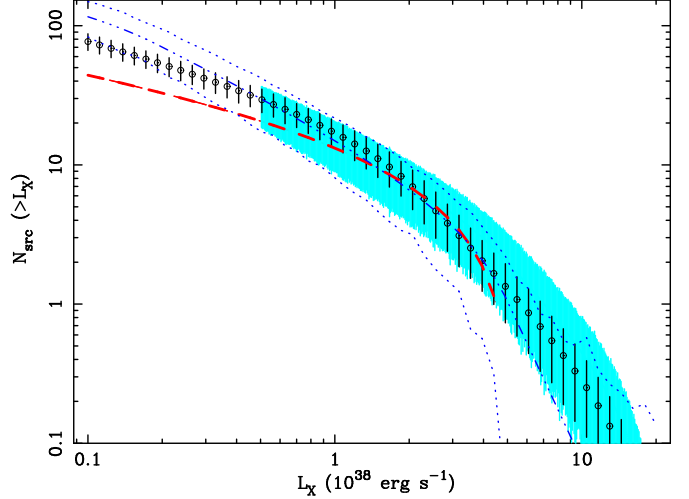


FIG. 14.— A comparison of our preferred *cumulative* XLF model (circles; black). The error-bars denote the approximate $1-\sigma$ uncertainty region) with other XLFs from the literature. We have normalized the model to match the observed number of sources with $L_X > L_{break}$ in the Milky Way. We compare it with the cumulative XLF of Galactic LMXBs from Grimm et al. (2002) (dashed line; red). We have corrected this model for the difference in energy-bands used between these authors and our work, under the assumption of a powerlaw spectrum with $\Gamma = 2.0$. We also compare to the “universal” LMXB XLF from Gilfanov (2004, blue; dash-dot-dot line), with the blue dotted lines delineating the approximate $1-\sigma$ uncertainty region for the models. We also show the best-fitting composite XLF for Kim & Fabbiano (2004, light blue shaded region). The latter two models have been scaled arbitrarily for clarity. We truncate both our model and that of Kim & Fabbiano above $2 \times 10^{39} \text{ erg s}^{-1}$. Model curves are only shown corresponding to luminosity ranges over which there were data to constrain the model. There is, in general, good agreement between the different models.

of our results which depend on the XLF shape (for incompleteness correction) do not appear to change qualitatively if we adopt an alternative XLF shape which is much steeper at low luminosities.

There is some evidence in our results that there is real scatter in the shapes of the XLF. In order to investigate this further, we considered the very deep XLFs determined in a few individual cases. Voss & Gilfanov (2006) report an XLF for Cen A which shows a clear flattening below $5 \times 10^{37} \text{ erg s}^{-1}$; the low- L_X β is comparable to our measurements. Although it is difficult to interpret a cumulative XLF due to the strong correlations between data-points, it is interesting to note that NGC 3379 shows a significantly flatter XLF at low L_X than $\beta = 2$ (Kim et al. 2006a), which would also be consistent with our broken powerlaw model. Possible counter-examples, however, include M 87, in which the XLF can be fitted as a broken powerlaw but with $\beta_1 \sim 2$ (Jordán et al. 2004). Fitting a differential (rather than cumulative) XLF compiled from these authors’ published source luminosities, we confirm this result, and find that our best fit to the composite XLF is marginally rejected. Kim et al. (2006a) find an XLF for NGC 4278 which similarly appears to resemble an unbroken powerlaw, with $\beta \sim 2$. These results provide further evidence that there is genuine scatter in the shapes of the XLFs between individual galaxies, in particular at low luminosities. On average, though, we have shown that it must flatten at low L_X . Clearly further, deep studies of the LMXB XLF in more galaxies are needed to investigate the origin of the scatter.

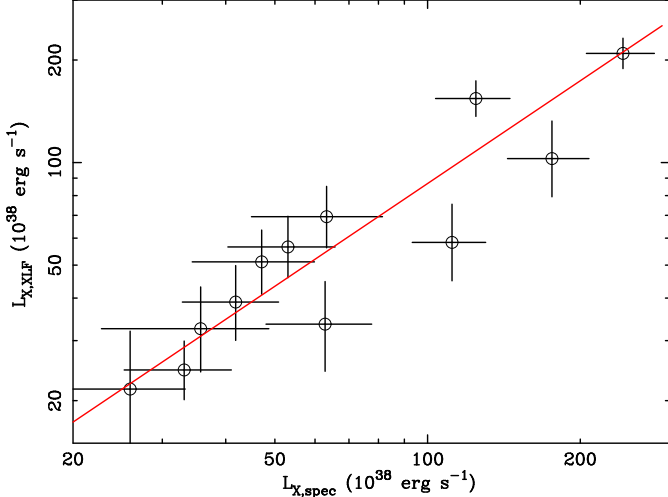


FIG. 15.— A comparison between the X-ray luminosity of point-sources determined from spectral-fitting ($L_{\text{X,spec}}$) and that determined from fitting the XLF ($L_{\text{X,XLF}}$) *within the same region* (see text). The best-fitting linear relation is shown.

6.1.2. The total luminosity of LMXBs

In the present work, we chose to estimate the luminosity of the total LMXB populations by extrapolation down to $10^{37} \text{ erg s}^{-1}$. This is, in part, justified by the excellent agreement, at least to this luminosity, between our best-fitting composite XLF and that of LMXBs in the Milky Way (Fig 14). Another way to test the validity of this assumption is to adopt a procedure similar to that outlined in Irwin (2005). The ensemble average of LMXBs which are too faint to have been detected individually should contribute a hard component to the spectrum of the diffuse emission in each galaxy. Therefore we extracted, for each galaxy, a spectrum from the region in which the XLF is computed (excluding regions around all detected point sources), and added the luminosity of the hard (unresolved LMXBs) component to the the combined luminosity of the detected sources. The details of the spectral extraction procedure and the treatment of the background are given in Humphrey & Buote (2006).

In practice, however, the procedure is rather complex for a number of reasons. First, some fraction of the point-sources are actually interloper AGNs. All sources with apparent $L_{\text{X}} > 2 \times 10^{39} \text{ erg s}^{-1}$ were assumed to be interlopers but, to minimize the effects of cosmic variance (which is dominated by the rare, bright point-sources), we disregarded these entirely. We estimated the expected *apparent* luminosity of interlopers over the flux range of interest from the model of Tozzi et al. (2001), and took into account the fraction of the expected flux which had been accounted for by the cosmic X-ray background component in our background modelling. Since the LMXB emission arises from a finite number of discrete sources, Poissonian statistics actually introduces an *intrinsic* uncertainty into the combined luminosity of these objects, irrespective of how accurately we can measure the total L_{X} . We estimated the magnitude of this uncertainty *via* Monte-Carlo simulations, in which a fixed number of sources were randomly drawn from a luminosity distribution matching the measured XLF, and the total luminosity measured. For each set of simulations, we were able to estimate the scatter (standard deviation) in the

total luminosity as a function of its expected value. For each galaxy, the scatter was added in quadrature with the measurement errors.

Fig 15 shows a comparison of the luminosity determined from XLF fitting ($L_{\text{X,XLF}}$) and that determined from the above procedure ($L_{\text{X,spec}}$). In a significant fraction of the galaxies, we found that $L_{\text{X,spec}}$ was extremely sensitive to the modelling or treatment of the background (consistent with the assessment of the systematic error budget in Humphrey & Buote 2006), and so these galaxies have been omitted from the comparison. In our analysis, the background is determined through a modelling procedure, which we have determined to be more reliable than adopting the background “templates”. We identified objects in which the modelling is likely suspect, at least in the crucial high-energy range, by examining the total flux of one of the modelled spectral components—the powerlaw, which accounts for the unresolved fraction of the X-ray background. Although this flux is subject to the effects of cosmic variance, we should be able to resolve out a significant fraction of the brightest background sources (which contribute most to the cosmic variance). Therefore, we should reasonably expect that the flux of this modelled component should be *lower* than the total flux of the AGN contribution to the background found by, for example, Tozzi et al. (2001), even accounting for cosmic variance. In half of the galaxies, we actually found that its flux was considerably higher than expected from this argument, typically indicating systems in which our models do not completely capture the shape of the high-energy background. In such circumstances, $L_{\text{X,spec}}$ is almost certainly in error (even though the luminosity of the hot gas emission, which has a much softer spectrum, is fairly well-determined), and so is omitted here.

We fitted a model of the form $L_{\text{X,XLF}} = \zeta L_{\text{X,spec}}$ to these data. Since the XLF certainly extends to fainter LMXBs than $10^{37} \text{ erg s}^{-1}$, we do not expect ζ to be exactly 1; its precise value depends on both the shape of the XLF and the actual low- L_{X} cut for LMXBs. Extrapolating our preferred XLF, for example, we expect ζ to be in the range 0.9–1.0. In contrast, for pure powerlaw XLF with $\beta = 2.0$, ζ may be as low as 0.70 if the XLF is unbroken down to $10^{36} \text{ erg s}^{-1}$. Computing $L_{\text{X,XLF}}$ for each galaxy with our best-fitting composite XLF, we obtained a good fit with this model ($\chi^2/\text{dof} = 11.1/11$), with $\zeta = 0.87 \pm 0.12$, which is consistent with expectations. Adopting $L_{\text{X,XLF}}$ from the powerlaw fits to the XLF, we found $\zeta = 1.06 \pm 0.16$, which implies that the XLF must be truncated below a limit which is $\gtrsim 5 \times 10^{36} \text{ erg s}^{-1}$.

Previous authors have reported a strong correlation between the total luminosity of the X-ray sources and the K-band luminosity of the galaxy (Gilfanov 2004; Kim & Fabbiano 2004). Using our larger sample of galaxies, we find a similar correlation (Fig 16), corresponding to

$$L_{\text{X}}^{\text{LMXB}}/L_{\text{K}} = 0.11 \times 10^{30} \text{ ergs}^{-1} L_{\text{K}\odot}^{-1} \quad (8)$$

with a scatter of $0.06 \times 10^{30} \text{ ergs}^{-1} L_{\text{K}\odot}^{-1}$, assuming our preferred XLF shape for each galaxy. For comparison, if we assumed that the XLF is a powerlaw with $\beta = 2.0$, the mean and scatter (omitting IC 4296, for which the error-bars are large) became $0.17 \times 10^{30} \text{ ergs}^{-1} L_{\text{K}\odot}^{-1}$ and

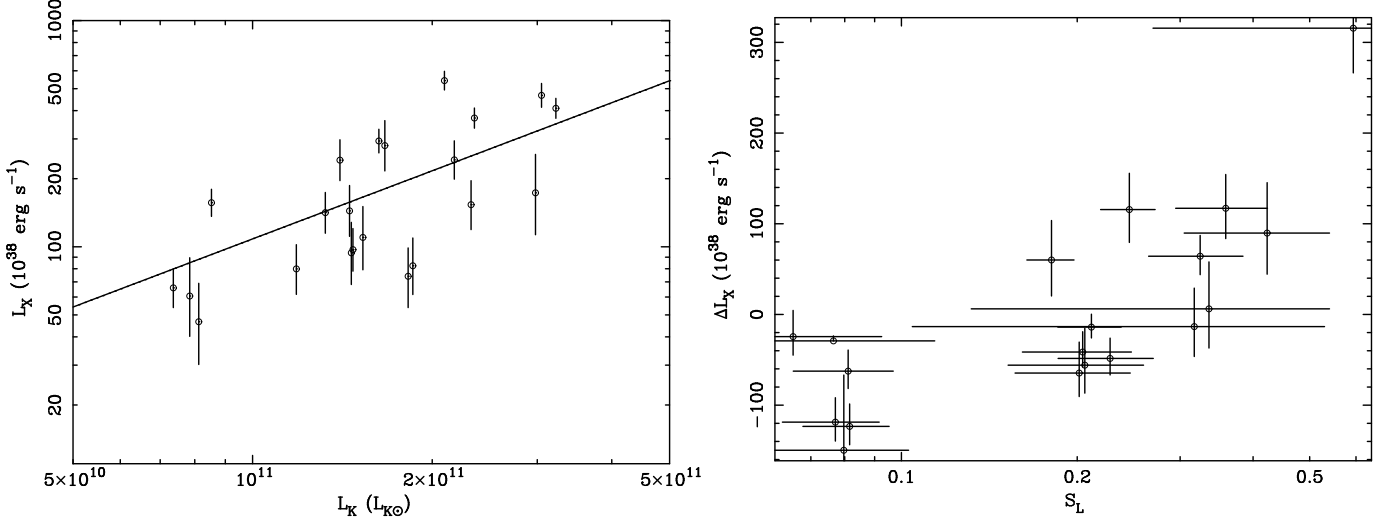


FIG. 16.— *Left:* The integrated luminosity of the LMXBs in the galaxies, shown as a function of K-band luminosity, adopting our preferred, broken powerlaw XLF. We also show the mean straight line relation. *Right:* The deviation of L_X from its the mean relation shown in the left panel *versus* S_L .

$0.09 \times 10^{30} \text{ ergs}^{-1} L_{K\odot}^{-1}$, respectively, in excellent agreement with Kim & Fabbiano (2004). In both cases the statistical errors are considerably smaller than the intrinsic scatter.

At face value this correlation indicates that the integrated LMXB population is a good indicator of the stellar mass in the galaxy (Gilfanov 2004). However, as we show in § 5.5, the majority, if not all, of the LMXBs must be formed in GCs. The relation between the numbers of LMXBs and the combined luminosity of the GCs does not show any scatter larger than the (albeit large) statistical errors. There is, however, a correlation between luminosity and the numbers of GCs in a galaxy suggesting that the correlation found in Fig 16 may arise through this third parameter. We show in the right panel of Fig 16 the deviation of L_X from the mean relation with respect to L_K as a function of S_L . This shows a clear correlation, which would support this interpretation, although this figure should be treated with caution since S_L and L_X are not computed from self-consistent apertures.

6.1.3. The high- L_X slope

Given the quality of the data, it was not possible to investigate how L_{break} or β_1 vary between galaxies. However, we were able to investigate whether β_2 , the high- L_X slope, does so, possibly providing further clues as to the origin of the XLF shape. Where it could be constrained, we allowed β_2 to fit freely and the results are shown in Table 3. We searched for correlations between it and various interesting parameters such as age, metallicity and $[\alpha/\text{Fe}]$ for the stellar population, S_L and the peak colour of the GC distribution. The ages and metallicities listed in Table 1 were computed as described in Humphrey & Buote (2006) and Humphrey et al. (2006). For those systems for which the age had been fixed to 12 Gyr in our previous analysis we relaxed this constraint when estimating the age.

If the high-luminosity sources are dominated by short-lived objects forming in the field (e.g. Wu 2001), we would expect to see a correlation between β_2 and the stellar age. Ivanova & Kalogera (2006) constructed a

model for the high- L_X XLF slope, which they related to the transient duty cycle. In this picture, if mass-transfer is dominated by red giant or white dwarf donors, β_2 should also depend on age. However, we did not find any evidence of a correlation ($\text{prob}(\text{no correlation})=70\%$ for Kendal's τ -test, and we obtained similar results with Spearman's rank test) between β_2 and age (Fig 17).

In contrast we did find a marginally significant correlation between $[\alpha/\text{Fe}]$ and β_2 , as shown in Fig 17, for which $\text{prob}(\text{no correlation})=3-8\%$ for the different tests. To investigate whether such a correlation is robust in the presence of the large statistical errors, we investigated the effect of randomly scattering the data-points within their error-bars. We found that 56% of the resulting simulations gave a significant correlation (in comparison to the 5% expected if the correlation is not robust). Given the number of different trials we performed, the correlation between $[\alpha/\text{Fe}]$ and β_2 should be considered tentative at best, and needs to be confirmed with a larger data-set. Nonetheless, taking it at face value, it is intriguing. One possible cause of such a correlation is a systematically-varying IMF. A more top-heavy IMF would increase $[\alpha/\text{Fe}]$ and also affect the compact object demographics. If there are more massive objects, it is unsurprising if more sources are observed which are able to sustain high L_X . Alternatively, enhanced $[\alpha/\text{Fe}]$ in the stars may significantly affect how mass transfer operates, increasing the population of X-ray bright LMXBs. However, neither the peak GC colour nor overall metallicity appear to correlate with β_2 , and it is not clear why $[\alpha/\text{Fe}]$ should have a stronger impact on the accretion process than total metallicity. Clearly both of these scenarios require that either the high- L_X sources are systematically biased to form in the field (since most LMXBs do not), or the variations in stellar $[\alpha/\text{Fe}]$ (and/ or the IMF) must also be reflected in the GC populations.

6.1.4. The meaning of the break

Early results suggesting the presence of an XLF break at $\sim 2 \times 10^{38} \text{ erg s}^{-1}$ have been called into question due to the failure of the authors to correct properly for source detection incompleteness (Kim & Fabbiano 2004).

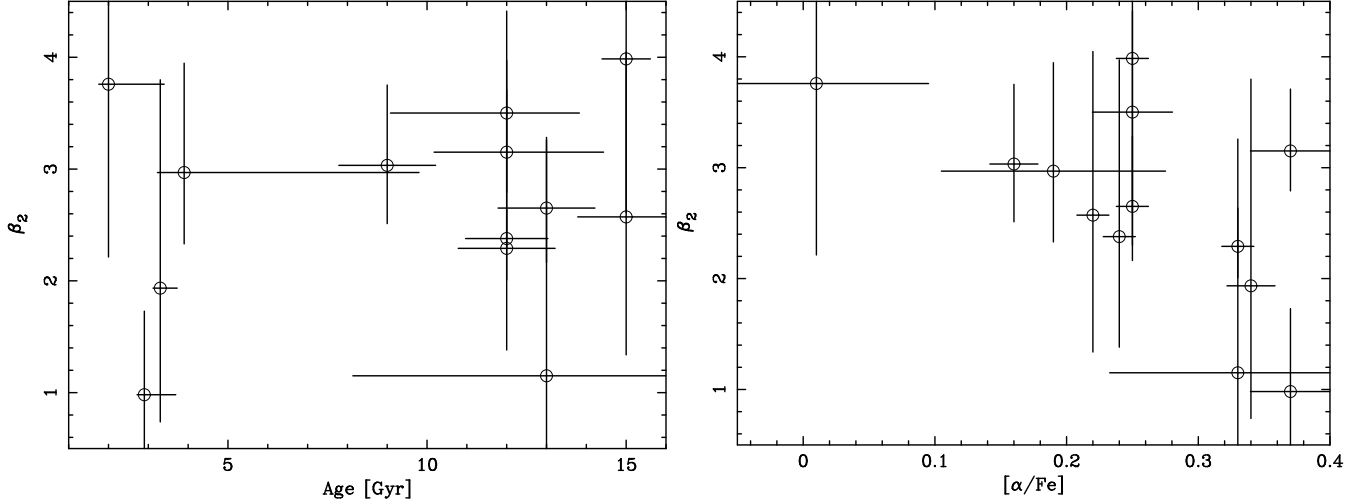


FIG. 17.— The slope of the XLF at $L_X > 2 \times 10^{38} \text{ erg s}^{-1}$ versus age (left panel) and $[\alpha/\text{Fe}]$ (right panel) of the stellar populations.

Although we now confirm the presence of such a break even when the data have been corrected for incompleteness, *a break was not required statistically in any individual galaxy*. The significance of the feature in some early analyses may have been exaggerated, therefore, by incompleteness effects.

It has been suggested (Sarazin et al. 2001) that the break represents a division between neutron-star and black-hole binary systems, with objects above this limit being entirely black hole binaries, and those below the limit a mixture of black hole binaries and neutron-stars. It is difficult to reconcile this hypothesis, however, with the shape of the XLF. Most systems are not observed close to their Eddington limit; for example all neutron-star LMXBs do not have $L_X \sim 2 \times 10^{38} \text{ erg s}^{-1}$. Therefore, the black-hole binary XLF would be expected to extend below this limit and, crucially, would not be expected to exhibit any feature at this characteristic luminosity. An extrapolation of the high- L_X slope (comprising only the putative black hole population) dramatically over-estimates the numbers of sources at low L_X , since the XLF *flattens* below the break, effectively ruling out this picture. Although Sarazin et al. (2001) actually recognized this problem, they argued there must be different source populations either side of the break. However, this would still, in fact, require the black hole binary XLF to “care” about the Eddington limit of a neutron-star, which is not expected. Bildsten & DeLooye (2004) explained both the break and low- L_X slope of the XLF found by Kim & Fabbiano (2004) in terms of ultra-compact X-ray binaries. However, the break luminosity we detect is significantly lower and, more problematically, the low- L_X slope predicted ($\beta \sim 1.8$) is much steeper than we detect.

It is worth noting that a further problem with interpreting the break as the Eddington limit is, of course, that the point source L_X we measure in the *Chandra* band is certainly an underestimate of the bolometric luminosity. For example, for the representative Galactic neutron-star X-ray binaries X 1916-053 and X 1624-490, an extrapolation of the best-fitting models for broad-band BeppoSAX observations (Church et al. 1998; Balucińska-Church et al. 2000) implies the 0.3–7.0 keV flux under-

estimates that in the 0.1–200 keV band by factors ~ 2.8 and 1.5, respectively, and obviously the bolometric flux is underestimated by even larger factors.

Another possible explanation for the break is that it arises from an evolving LMXBs population born in a putative recent burst of star formation (Jeltema et al. 2003; Wu 2001). The absence of any obvious correlation between the high- L_X shape and the age of the stars seems to rule out this model. Furthermore, given the short lifetime of an X-ray binary ($\lesssim 10^8 \text{ yr}$) this model seems unlikely to be able to sustain a break at $2 \times 10^{38} \text{ erg s}^{-1}$ in a typical galaxy with a $\sim 12 \text{ Gyr}$ stellar population. In any case, we did not find any convincing evidence of a break which systematically evolves from galaxy-to-galaxy and most, if not all, LMXBs are formed in GCs.

The well-studied population of Milky Way LMXBs provides some intriguing clues as to what may be the origin of the break. Galactic LMXBs are known to be highly variable (e.g. Liu et al. 2001; Grimm et al. 2002). In particular, all confirmed LMXB black hole binaries in the Milky Way are transient sources (McClintock & Remillard 2003), and there is evidence that a significant portion of LMXBs in early-type galaxies may also be transient (e.g. Kraft et al. 2001). Different classes of LMXB, which exhibit strikingly different patterns of variability occupy distinct luminosity bands (e.g. Hasinger & van der Klis 1989), so that the XLF is not expected to be “scale-free”. It is striking that the so-called “Z-track” sources, which comprise the majority of the most luminous persistent LMXBs in the Milky Way have $L_X \sim 1\text{--}3 \times 10^{38} \text{ erg s}^{-1}$ (Grimm et al. 2002), measured in the *Chandra* band, in good agreement with L_{break} in the early-type galaxy XLF. If, as in the Milky Way, sources brighter than this limit are predominantly lower- L_X sources exhibiting brief periods of outburst or flaring, this would naturally cause a break. This can be explicitly tested by looking for characteristic patterns of (spectral) variability in the brightest LMXBs. In the current work there were, unfortunately, insufficient photons to allow us to do this. One possible counter-argument to this picture is the observation by Irwin (2006) that no transient behaviour was seen in the brightest sources in NGC 1399 and M 87, over a timescale of \sim a few years,

effectively placing a limit on transient behaviour in these objects of ~ 50 yr. Although these objects are obviously not short-term transients, in no way does this work suggest they are *not* transient over periods of a few decades or longer, and so our interpretation still holds. In any case, such long-term transients appear very rare (as seen in the Milky Way).

As a corollary, it is interesting to note that source variability may have other impacts on the shape of the XLF. The characteristic patterns of short term variability (e.g. White et al. 1995) are superimposed on long term secular evolution in the mass-transfer rate (e.g. Podsiadlowski et al. 2002), so that the locus of an individual source in the XLF should evolve with time. It is possible, therefore, that the time-averaged lightcurve may be the dominant factor in determining the shape of the XLF, which might explain the comparative uniformity in its shape from galaxy to galaxy. Obviously compact object demographics must play a role since black-hole binary systems exhibit, on average, slightly different properties to neutron-star systems (Tanaka & Lewin 1995). Therefore differences in the IMF might still produce the possible correlation we see between $[\alpha/\text{Fe}]$ and β_2 .

6.2. The GC-LMXB connection

We find a strong correlation between the number of GCs in the galaxy and the number of LMXBs, placing tight constraints on the fraction of sources formed in the field. We find that the number of LMXBs formed in the field is $< 1.8 \times 10^{-10} L_V / L_{V\odot}$, implying $\lesssim 10\%$ of the LMXBs in a galaxy with $S_L \sim 0.2$. In fact, the data are consistent with the hypothesis that *all* the LMXBs are formed within GCs. Ideally we would have performed this comparison using the K-band, rather than the V-band light, since it better traces the mass of the underlying stellar population. However, since our best-fitting relation passes through the origin, this indicates the number of LMXBs is consistent with being exactly proportional to the combined V-band luminosity of the GCs. Since the GCs are expected to be uniformly old stellar systems (e.g.. Paper II), the V-band mass-to-light ratio should not vary considerably between the galaxies. Scaling both the number of LMXBs and the luminosity of GCs for each galaxy by the same arbitrary factor (e.g. the K-band luminosity of the galaxy; hence computing $S_{N,X}$ and S_L using the K-band, rather than V-band luminosity) should not affect the quality of a “y \propto x” fit to the data. Although the exact numerical relations we derive depend on the shape of the XLF we adopt for incompleteness correction, qualitatively our conclusions are found to be insensitive to the exact XLF shape.

Our conclusions are significantly different from those of Irwin (2005), who, using a smaller sample of galaxies, argued that the total *luminosity* of the LMXBs divided by the optical luminosity of the galaxy is proportional to S_N *plus a constant offset*. We suspect the reason for this discrepancy arises from the way in which the luminosity of undetected LMXBs was estimated. Irwin (2005) computed the luminosity of unresolved LMXBs from the high-energy (2.0-6.0 keV) portion of the diffuse emission spectrum in each galaxy (excepting NGC 1399). This implicitly assumes that there is no contribution from the hot ISM at these energies, which for a number of the galaxies in the sample may not be strictly

true (e.g. Humphrey & Buote 2006; Humphrey et al. 2004). More problematically, the determination of the unresolved source flux from the spectrum is very sensitive to the treatment of the background (§ 6.1.2). Although Irwin took a local background from the outer parts of the S3 chip, this fundamentally requires that there is no extended diffuse emission in any of the galaxies, which is not true for all of the galaxies in the sample (e.g. Humphrey et al. 2004), and requires careful treatment of vignetting effects. In fact, he found that, when attempting spectral fitting, the models systematically underestimated the high-energy spectrum, in contrast to our results when carefully modeling the background (Humphrey & Buote 2006), suggesting that the background may not have been completely accounted for.

We found that ~ 1 currently active ($L_X > 10^{37} \text{ erg s}^{-1}$) LMXB was formed per $10^6 L_\odot$ V-band integrated luminosity of GCs, of which $\sim 40\text{--}50\%$ of the LMXBs are retained within the GC. Approximately 7% of the GCs within the WFPC2 field contain an active LMXB, in rough agreement with the fraction seen in the Milky Way and, possibly, M31 (Di Stefano et al. 2002). If the lifetime of an LMXB is τ_L and the fraction of the time it is active with $L_X > 10^{37} \text{ erg s}^{-1}$ is F_d , our results imply an LMXB formation rate in GCs of $\sim 10^{-14} L_{V\odot}^{-1} \text{ yr}^{-1} (\tau_L / 10^8 \text{ yr})^{-1} F_d^{-1}$, or $\sim 1.5 \text{ Gyr}^{-1} (\tau_L / 10^8 \text{ yr})^{-1} F_d^{-1}$ per GC, averaging over the mean GCLF.

Another piece of evidence which supports the hypothesis that all LMXBs form in GCs is the good agreement between the spatial distribution of the LMXBs and the GCs, when one considers an appropriately-weighted combination of the red and blue GCs. We find no evidence of a difference in the spatial distributions of LMXBs found in GCs and the field implying that field LMXBs are most likely ejected only with modest kick velocities from GCs. With a smaller sample of galaxies Kim et al. (2006b) found similarities in the distributions of the LMXBs in the field and in GCs, consistent with our result, but found that the LMXB distribution was far steeper than the GCs. These authors’ optical data covered a larger radial range than ours, and so it is possible the agreement we find with our data is an artifact of our smaller field of view. However, we note that these authors did not correct for the spatial variation in source detection incompleteness, which affects radial profiles of both the LMXBs and the GCs, and may have played a role in this discrepancy. In contrast Kundu et al. (2007) report, based on a sample of 5 galaxies, that the LMXB-hosting GCs are distributed similarly to the GCs, whereas field LMXBs have a more centrally-peaked distribution. To some extent, we suspect that small number statistics also plays a role in the discrepancies between these authors’ work and ours. The sample of Kundu et al. (2007), for example, contains the S0 galaxy NGC 3115, which had the most centrally-peaked LMXB distribution in our sample. Furthermore, these authors compare the distribution of LMXBs and that of *all* the GCs, which is more extended than an appropriately-weighted combination of red and blue GCs (see § 5.3).

Having corrected for source detection incompleteness in both the LMXB and GC populations, we found little evidence that the fraction of LMXBs coincident with

GCs vary from galaxy to galaxy. This is in sharp contrast to past studies (Juett 2005), which argued for a correlation between this fraction and the specific frequency of globular clusters, which implies a significant fraction of the LMXBs are formed in the field. This study, however, drew upon literature results which did not always treat the data consistently. In particular, literature values of S_N were used, which were typically not computed in the same aperture as was used for LMXB-GC matching. Since the distribution of GCs as a whole is flatter than the optical light (or the distribution of LMXBs, which follow the more centrally-peaked red GC distribution), it is crucial that S_N is computed within this aperture. Adopting locally-computed specific frequencies the correlation of Juett is seriously degraded, as pointed out by Kim et al. (2006b). Furthermore, when one corrects for incompleteness, there is little evidence of any statistically significant variation from galaxy-to-galaxy.

We found that the probability a given GC contains an LMXB is proportional to its luminosity to the power of 1.01 ± 0.19 and its metallicity to the power of 0.33 ± 0.11 . These values are very similar to recent results obtained by Sivakoff et al. (2007), Jordán et al. (2004, for M 87) and the sample of Smits et al. (2006). In order to interpret these results in terms of physical models, it is necessary to recast Eqn 2 in terms of M_{GC} , the mass of the GC. For the range of stellar metallicities implied by the colours of LMXB-hosting GCs ($[Fe/H] \sim -1.6\text{--}0.25$), the stellar M/L_V ratio actually depends on metallicity. To illustrate this point, we adopted M/L_V ratios for an assumed 10 Gyr population with a Kroupa IMF from Maraston (1998)⁴ and found $M/L_V \sim 3.5 Z_{Fe}^{0.19}$, which is accurate to better than $\sim 10\%$ for the range of interest. Inserting this into Eqn 2, we obtained $P(GC, X) \simeq 0.023(M_{GC}/M_0)^{1.01 \pm 0.19}(Z_{GC}/Z_0)^{0.14 \pm 0.12}$, where $M_0 = 1.6 \times 10^5 M_\odot$.

Maccarone et al. (2004) proposed an irradiation-induced wind model to account for an excess of red GCs harbouring LMXBs, which predicts an approximately powerlaw dependence on metallicity, with an exponent ~ 0.39 . This is stronger than the dependence we obtained (differing at $\sim 2\sigma$). Furthermore, we note that the predicted enhanced absorption in the blue-GC LMXBs than red-GC LMXBs is not observed in our data. It is interesting to note that Maccarone et al. (2004) also estimated that the effects of metallicity on stellar radius should lead to a dependence $P(GC, X) \propto Z_{GC}^{0.12}$, which is in good agreement with our estimate above. We stress that our value of the metallicity exponent is derived assuming that all of the colour variation between GCs arises solely from metallicity effects, ignoring the effects of age, which would affect both the M/L ratio and the conversion from GC colour to metallicity. Clearly further multi-colour or deep spectroscopic observations to break the age-metallicity degeneracy are needed to investigate this further.

7. SUMMARY AND CONCLUSIONS

Using a sample of 24 galaxies observed with *Chandra* we found, in summary:

⁴ Using the updated model-grids made available by the author at http://www-astro.physics.ox.ac.uk/~maraston/Stellar_Population_Models.html

1. Correcting for source detection incompleteness, the point-source XLF of individual galaxies is consistent with a single powerlaw, with $\beta \sim 2.0$. We find that β correlates with incompleteness, indicating that the XLF steepens at low L_X .
2. The composite XLF of all the galaxies is best-fitted by a broken powerlaw with a break at $2.21_{-0.56}^{+0.65} \times 10^{38} \text{ erg s}^{-1}$ and slopes $1.40_{-0.13}^{+0.10}$ and $2.84_{-0.30}^{+0.39}$ above and below the break, respectively.
3. The shape of the XLF is inconsistent with the break representing a strict division between black hole and neutron-star systems. However, in common with the Milky Way, it may represent the luminosity of the brightest persistent LMXB, so that sources with higher L_X are exhibiting flaring or in transient outburst, naturally producing a break.
4. The slope of the XLF at high luminosities does not correlate with the stellar population age, but shows evidence of a weak correlation with $[\alpha/\text{Fe}]$, suggesting a possible effect of the IMF on the XLF.
5. We found that the combined LMXB luminosity is approximately proportional to L_K of the galaxy. However, there is significant intrinsic scatter in the relation, such that L_X^{LMXB}/L_K has a mean and standard deviation of 0.11 and $0.06 \times 10^{30} \text{ ergs}^{-1} L_K^{-1}$.
6. We find no difference in the XLF or composite spectra between LMXBs in GCs and those in the field. LMXBs in red and blue GCs have essentially the same spectrum, ruling out the irradiation induced model of Maccarone et al. (2004).
7. Correcting for incompleteness, GC colour and GCLF effects, we find that the probability a GC hosts an LMXB with $L_X > 10^{37} \text{ erg s}^{-1}$ is $\sim 6.5\%$, and the probability an LMXB is in a GC is $\sim 40\%$. These do not vary from galaxy to galaxy.
8. The probability that a GC hosts an LMXB depends on luminosity and metallicity to the powers $\alpha = 1.01 \pm 0.19$ and $\gamma = 0.33 \pm 0.11$, respectively. When the metallicity dependence of the stellar M/L ratio is taken into account, the tendency for red GCs preferentially to host LMXBs may be consistent solely with metallicity influences on stellar radii.
9. The specific frequency of LMXBs is proportional to the S_L without a significant constant offset, implying that all LMXBs form in GCs. Our results imply an LMXB formation rate of $\sim 1.5 \text{ Gyr}^{-1} (\tau_L/10^8 \text{ yr})^{-1} F_d^{-1}$ per GC (where τ_L is the LMXB lifetime and F_d the fraction of its life spent with $L_X > 10^{37} \text{ erg s}^{-1}$), and put an upper limit of $\sim 1.8 \times 10^{-10} L_V/L_{V\odot}$ LMXB with $L_X > 10^{37} \text{ erg s}^{-1}$ formed in the field.
10. This is further supported by the fact that the LMXB distribution closely follows the distribution of red GCs, when incompleteness is taken into account. Furthermore, the spatial distributions of GC and field LMXBs are essentially the same.

11. With the present data we cannot completely rule out that the two galaxies which dominate the XLF at the lowest L_X are not representative, which could distort the XLF shape in that region. Although this would have an impact on our numerical results, qualitatively our conclusions appear insensitive to the low- L_X slope.

We would like to thank Fabio Gastaldello and Luca Zappacosta for interesting discussions. We would also like to thank Jimmy Irwin for providing comments on the draft, and Rasmus Voss for discussions. This research has

made use of data obtained from the High Energy Astrophysics Science Archive Research Center (HEASARC), provided by NASA's Goddard Space Flight Center. In addition, we made use of data obtained from the MAST archive. This research has also made use of the NASA/IPAC Extragalactic Database (*NED*) which is operated by the Jet Propulsion Laboratory, California Institute of Technology, under contract with NASA, and the HyperLEDA database (<http://leda.univ-lyon1.fr>). Support for this work was provided by NASA under grant NNG04GE76G issued through the Office of Space Sciences Long-Term Space Astrophysics Program.

APPENDIX SOURCE LISTS

We include in Table 6 the point-source lists of all the galaxies in the sample. We include only those sources within D_{25} of each galaxy, which should mitigate against contamination by background AGN. For each source, we provide the source name, which incorporates the coordinate information, the total number of counts detected, the 0.3–7.0 keV X-ray luminosity (L_X), the two hardness ratios HR1 and HR2 (§ 3.1) and the projected distance from the galaxy centre (Δ_R). For those LMXBs within the appropriate WFPC2 field, we list under “GC” the GC catalogue number given in Paper II for any which match GCs. If the source has no match, we report “None”, and if the source is not in the WFPC2 field, it is marked by an ellipsis.

REFERENCES

Angelini, L., Loewenstein, M., & Mushotzky, R. F. 2001, *ApJ*, 557, L35
 Bałucińska-Church, M., Humphrey, P. J., Church, M. J., & Parmar, A. N. 2000, *A&A*, 360, 583
 Belczynski, K., Kalogera, V., Zezas, A., & Fabbiano, G. 2004, *ApJ*, 601, L147
 Bellazzini, M., Pasquali, A., Federici, L., Ferraro, F. R., & Pecci, F. F. 1995, *ApJ*, 439, 687
 Bildsten, L. & Deloye, C. J. 2004, *ApJ*, 607, L119
 Blanton, E. L., Sarazin, C. L., & Irwin, J. A. 2001, *ApJ*, 552, 106
 Church, M. J. & Bałucińska-Church, M. 2001, *A&A*, 369, 915
 Church, M. J., Parmar, A. N., Bałucińska-Church, M., Oosterbroek, T., dal Fiume, D., & Orlandini, M. 1998, *A&A*, 338, 556
 Clark, G. W. 1975, *ApJ*, 199, L143
 Colbert, E. J. M., Heckman, T. M., Ptak, A. F., Strickland, D. K., & Weaver, K. A. 2004, *ApJ*, 602, 231
 Davis, J. E. 2001, *ApJ*, 548, 1010
 de Vaucouleurs, G., de Vaucouleurs, A., Corwin, H. G., Buta, R. J., Paturel, G., & Fouque, P. 1991, Third Reference Catalogue of Bright Galaxies (Volume 1-3, XII, 2069 pp. 7 figs.. Springer-Verlag Berlin Heidelberg New York)
 Di Stefano, R., Kong, A. K. H., Garcia, M. R., Barmby, P., Greiner, J., Murray, S. S., & Primini, F. A. 2002, *ApJ*, 570, 618
 Dickey, J. M. & Lockman, F. J. 1990, *ARA&A*, 28, 215
 Fabbiano, G. 1989, *ARA&A*, 27, 87
 Fabbiano, G. 2006, *ARA&A*, 44, 323
 Faber, S. M., Wegner, G., Burstein, D., Davies, R. L., Dressler, A., Lynden-Bell, D., & Terlevich, R. J. 1989, *ApJS*, 69, 763
 Fabian, A. C., Pringle, J. E., & Rees, M. J. 1975, *MNRAS*, 172, 15P
 Freeman, P. E., Kashyap, V., Rosner, R., & Lamb, D. Q. 2002, *ApJS*, 138, 185
 Gebhardt, K. & Kissler-Patig, M. 1999, *AJ*, 118, 1526
 Giacconi, R., Gursky, H., Paolini, F. R., & Rossi, B. B. 1962, *Phys. Rev. Lett.*, 9, 439
 Gilfanov, M. 2004, *MNRAS*, 349, 146
 Grimm, H.-J., Gilfanov, M., & Sunyaev, R. 2002, *A&A*, 391, 923
 Grimm, H.-J., Gilfanov, M., & Sunyaev, R. 2003, *MNRAS*, 339, 793
 Grindlay, J. E. 1987, in IAU Symposium, Vol. 125, The Origin and Evolution of Neutron Stars, ed. D. J. Helfand & J.-H. Huang, 173–184
 Hasinger, G. & van der Klis, M. 1989, *A&A*, 225, 79
 Humphrey, P. J. 2008, *ApJ*, submitted
 Humphrey, P. J. & Buote, D. A. 2004, *ApJ*, 612, 848
 Humphrey, P. J. & Buote, D. A. 2006, *ApJ*, 639, 136
 Humphrey, P. J., Buote, D. A., & Canizares, C. R. 2004, *ApJ*, 617, 1047
 Humphrey, P. J., Buote, D. A., Gastaldello, F., Zappacosta, L., Bullock, J. S., Brighenti, F., & Mathews, W. G. 2006, *ApJ*, 646, 899
 Humphrey, P. J., Fabbiano, G., Elvis, M., Church, M. J., & Bałucińska-Church, M. 2003, *MNRAS*, 344, 134
 Irwin, J. A. 2005, *ApJ*, 631, 511
 Irwin, J. A. 2006, *MNRAS*, 371, 1903
 Irwin, J. A., Athey, A. E., & Bregman, J. N. 2003, *ApJ*, 587, 356
 Ivanova, N. 2006, *ApJ*, 636, 979
 Ivanova, N. & Kalogera, V. 2006, *ApJ*, 636, 985
 Jarrett, T. H. 2000, *PASP*, 112, 1008
 Jeltema, T. E., Canizares, C. R., Buote, D. A., & Garmire, G. P. 2003, *ApJ*, 585, 756
 Jensen, J. B., Tonry, J. L., Barris, B. J., Thompson, R. I., Liu, M. C., Rieke, M. J., Ajhar, E. A., & Blakeslee, J. P. 2003, *ApJ*, 583, 712
 Jordán, A., Côté, P., Ferrarese, L., Blakeslee, J. P., Mei, S., Merritt, D., Milosavljević, M., Peng, E. W., Tonry, J. L., & West, M. J. 2004, *ApJ*, 613, 279
 Juett, A. M. 2005, *ApJ*, 621, L25
 Kilgard, R. E., Kaaret, P., Krauss, M. I., Prestwich, A. H., Raley, M. T., & Zezas, A. 2002, *ApJ*, 573, 138
 Kim, D. .. et al. 2006a, *ApJ*, 652, 1090
 Kim, D. & Fabbiano, G. 2003, *ApJ*, 586, 826
 Kim, D. & Fabbiano, G. 2004, *ApJ*, 611, 846
 Kim, E., Kim, D.-W., Fabbiano, G., Lee, M. G., Park, H. S., Geisler, D., & Dirsch, B. 2006b, *ApJ*, 647, 276
 Kraft, R. P., Kregenow, J. M., Forman, W. R., Jones, C., & Murray, S. S. 2001, *ApJ*, 560, 675
 Kroupa, P. 2002, *Science*, 295, 82
 Kundu, A., Maccarone, T. J., & Zepf, S. E. 2002, *ApJ*, 574, L5
 Kundu, A., Maccarone, T. J., & Zepf, S. E. 2007, *ApJ*, in press, astro-ph/0703092
 Kundu, A., Maccarone, T. J., Zepf, S. E., & Puzia, T. H. 2003, *ApJ*, 589, L81
 Kundu, A. & Whitmore, B. C. 1998, *AJ*, 116, 2841
 Kundu, A. & Whitmore, B. C. 2001, *AJ*, 121, 2950
 Liu, Q. Z., van Paradijs, J., & van den Heuvel, E. P. J. 2000, *A&AS*, 147, 25
 Liu, Q. Z., van Paradijs, J., & van den Heuvel, E. P. J. 2001, *A&A*, 368, 1021

TABLE 6
LMXB SOURCE LISTS

Source	Counts	L_X (10^{38} erg s $^{-1}$)	HR1	HR2	Δ_R ($''$)	GC
IC 4296						
CXOU J133638.2-335755	27.	26. \pm 12.	0.43 \pm 0.26	0.66 \pm 0.49	0.17	...
CXOU J133639.4-335713	25.	24. \pm 10.	0.16 \pm 0.27	0.68 \pm 0.40	0.74	...
CXOU J133639.7-335751	17.	19. \pm 12.	0.31 \pm 0.60	-0.30 \pm 0.53	0.18	...
...

NOTE. — Catalogue of detected sources in each galaxy (see text). The full version of this table is available in the electronic version of the paper.

Maccarone, T. J., Kundu, A., & Zepf, S. E. 2004, ApJ, 606, 430
 Maraston, C. 1998, MNRAS, 300, 872
 McClintock, J. E. & Remillard, R. A. 2003, in Compact Stellar X-ray Sources, ed. W. H. G. Lewin & M. van der Klis (C.U.P.), astro-ph/0306213
 Paczyński, B. 1983, ApJ, 267, 315
 Podsiadlowski, P., Rappaport, S., & Pfahl, E. D. 2002, ApJ, 565, 1107
 Press, W. H., Teukolsky, S. A., Vetterling, W. T., & Flannery, B. P. 1992, Numerical Recipes in C: The Art of Scientific Computing. Second Ed. (C.U.P.)
 Sarazin, C. L., Irwin, J. A., & Bregman, J. N. 2000, ApJ, 544, L101
 Sarazin, C. L., Irwin, J. A., & Bregman, J. N. 2001, ApJ, 556, 533
 Sarazin, C. L., Kundu, A., Irwin, J. A., Sivakoff, G. R., Blanton, E. L., & Randall, S. W. 2003, ApJ, 595, 743
 Sivakoff, G. R., Jordán, A., Sarazin, C. L., Blakeslee, J. P., Côté, P., Ferrarese, L., Juett, A. M., Mei, S., & Peng, E. W. 2007, ApJ, 660, 1246
 Sivakoff, G. R., Sarazin, C. L., & Irwin, J. A. 2003, ApJ, 599, 218
 Smits, M., Maccarone, T. J., Kundu, A., & Zepf, S. E. 2006, A&A, 458, 477
 Tanaka, Y. & Lewin, W. H. G. 1995, in X-ray Binaries, ed. W. H. G. Lewin, J. van Paradijs, & E. P. J. van den Heuvel (C.U.P.), 126–171
 Tonry, J. L., Dressler, A., Blakeslee, J. P., Ajhar, E. A., Fletcher, A. A., Luppino, G. A., Metzger, M. R., & Moore, C. B. 2001, ApJ, 546, 681
 Tozzi, P., et al. 2001, ApJ, 562, 42
 Voss, R. & Gilfanov, M. 2006, A&A, 447, 71
 Wang, Q. D. 2004, ApJ, 612, 159
 White, N. E., Nagase, F., & Parmar, A. N. 1995, in X-ray Binaries, ed. W. H. G. Lewin, J. van Paradijs, & E. P. J. van den Heuvel (C.U.P.), 1–57
 White, R. E., Sarazin, C. L., & Kulkarni, S. R. 2002, ApJ, 571, L23
 Wu, K. 2001, Publications of the Astronomical Society of Australia, 18, 443
 Xu, Y., Xu, H., Zhang, Z., Kundu, A., Wang, Y., & Wu, X.-P. 2005, ApJ, 631, 809